Multiple losses of ecdysone receptor genes in nematodes: an alternative evolutionary scenario of molting regulation

Shumpei Yamakawa[1*], Lisa-Marie Barf[1], and Andreas Hejnol[1,2*]

1. Institute of Zoology and Evolutionary Research, Faculty of Biological Sciences, Friedrich Schiller University Jena, Jena, Germany

2. Department of Biological Sciences, University of Bergen, Bergen, Norway

*Corresponding authors: Andreas Hejnol, Shumpei Yamakawa

Email: andreas.hejnol@uni-jena.de, shumpei.yamakawa@gmail.com

ORCID: S.Y.: 0000-0002-2557-0670, L.-M.B: 0000-0001-7535-2690, A.H.: 0000-0003-2196-8507

Author Contributions: Conceptualization, S.Y..; methodology, S.Y. and L.-M.B.; software, S.Y. and L.-M.B.; formal analysis, S.Y.; investigation, S.Y and L.-M.B..; writing—original draft, S.Y.; writing—review & editing, S.Y., L.-M.B., and A.H.; visualization, S.Y.; funding acquisition, S.Y. and A.H.

Competing Interest Statement: The authors declare no competing interests.

Keywords: nematodes, ecdysone, molting, *ecr*, *nhr-23/hr3*.

Abstract

Molting is a hallmark feature of ecdysozoans, including arthropods, tardigrades, and nematodes. Ecdysone hormones play a crucial role in regulating the molting process of different ecdysozoan taxa. Interestingly, despite this highly conserved function of ecdysone, the model nematode *Caenorhabditis elegans* has lost the ecdysone receptor (ECR) genes and their molting appears to be ecdysone-independent. The loss of *ecr* has only been reported in *Caenorhabditis* within ecdysozoans, and the evolutionary background behind this loss has remained enigmatic. Here, we show that loss of *ecr* is not exceptional in *Caenorhabditis*, but has occurred at least three times in Rhabditina and Tylenchina nematodes. Our genome-wide analysis of 160 nematode species revealed multiple losses of *ecr* and its typical heterodimer partner *usp* during nematode evolution. Furthermore, using transcriptomic, pharmacological, and *in silico/ in vivo* protein interaction analyses, we identified two factors that potentially underlie and buffer the loss of ECR gene/function: (1) molting regulation by an alternative nuclear receptor HR3 (NHR-23) and (2) a lineage-specific expansion of nuclear receptors in the *ecr*-deficient taxa. Taken together, this study shows how key regulators of ecdysozoan molting can be altered during evolution. We propose a novel scenario for the evolution of molting regulation in nematodes.

Introduction

Ecdysozoa, which includes arthropods, nematodes, priapulids, and others, comprises more than 80% of all animal species (Aguinaldo, et al. 1997; Dunn, et al. 2008; Hejnol, et al. 2009). A defining feature of ecdysozoans is their ability to grow and change appearance by periodically shedding a cuticular exoskeleton (Nielsen 2012; Giribet and Edgecombe 2017; Schumann, et al. 2018). As the name Ecdysozoa derives from this unique growth strategy, molting or ecdysis (Aguinaldo, et al. 1997), the acquisition of a cuticular exoskeleton and molting process is a key innovation in ecdysozoan evolution. Despite its importance for understanding of ecdysozoan evolution, the evolutionary background of molting remains enigmatic.

Molting regulation has been well characterized in arthropods such as insects and decapods with ecdysone hormone as a master regulator (Fig. 1B) (Lachaise, et al. 1993; Thummel 1996; Yamanaka, et al. 2013; Niwa and Niwa 2014; Hyde, et al. 2019). In arthropods, ecdysone hormone is synthesized from cholesterol by a group of genes called the Halloween genes (e.g., *sad* and *phm*) in specific endocrine organs such as the prothoracic glands (Niwa and Niwa 2014). The secreted ecdysone is converted to 20-hydroxyecdysone (20E), which binds to the ecdysone receptor (ECR) in the target tissues (e.g., epidermal cells) (Yamanaka, et al. 2013). The ecdysone receptor (ECR) forms a heterodimer with another nuclear receptor USP to activate downstream cascade genes (e.g., HR3 and FTZ-F1, Fig. 1B) (Yamanaka, et al. 2013). Recently, we found that tardigrade molting is likely regulated by ecdysteroid hormone (Yamakawa and Hejnol 2024), suggesting that ecdysone-dependent molting is ancestral in panarthropods.

In nematodes, the developmental role of ecdysone hormone has been studied primarily in parasitic species (Fig. 1A and Table S1). For example, ecdysone and/or 20E have been detected in Rhabditina and Spirurina parasitic species, including *Haemonchus contortus*, *Anisakis simplex*, *Dirofilaria immitis*, and *Ascaris suum* (Fig. 1A, Table S1) (Fleming 1985; Cleator, et al. 1987; Evershed, et al. 1987; Fleming 1993). In *Ascaris suum*, 20E exhibits pulsatile fluctuations synchronized with the molting cycle, resembling patterns reported in arthropods (Fleming 1985). Pharmacological functional studies have

also been conducted to test whether ecdysone hormone regulates molting process (Fig. 1A and Table S1). Exogenous ecdysone or 20E treatment is reported to induce or prompt the molting of *Heligmosomoides polygyrus* (molting of L4 [4th larval stage] to adult), *Ascaris suum* (L4-adult), *Dirofilaria immitis* (L3-L4), and *Burgia malayi* (L3-L4) (Fig. 1A and Table S1) (Dennis 1976; Fleming 1985; Warbrick, et al. 1993; Mhashilkar, et al. 2016). Notably, Warbrick et al., 1993 showed that the ecdysone agonist RH5849 and antagonists Azadirachtin have a potential to induce and suppress L3-L4 molting of *D. immitis*, respectively. Similar to the pleiotropic functions of ecdysone in arthropods (Kozlova and Thummel 2000; Subramoniam 2000), effects of pharmacological treatment were also found in reproduction-related processes (ex., oocyte development in *D. immitis* and microfilarial release in *Brugia pahangi*) (Delves, et al. 1986; Barker, et al. 1991*)*. Finally, genetic components of ecdysone signaling, including ecdysone receptor and its heterodimer functionality, have also been identified in Rhabditina and Spirurina nematodes (Fig. 1A and Table S1) (Tzertzinis, et al. 2010). The above findings support the involvement of ecdysone hormone in the molting regulation of some nematode lineages such as Spirurina.

Interestingly, however, inconsistent results with ecdysone-dependent molting have been also reported in some nematode species (ex., no effects of ecdysone treatment in the molting of *Haemonchus contortus* (L3–L4) and *Meloidogyne javanica* (L2–L3) (Fig. 1A and Table S1) (Soriano, et al. 2004; Graham, et al. 2010). Remarkably, the model nematode *Caenorhabditis elegans* is known to lack any genes coding the ecdysone hormone receptor (ECR) (Schumann, et al. 2018; Taubenheim, et al. 2021). As *ecr* has been identified in different nematode taxa (Shea, et al. 2004; Graham, et al. 2010; Parihar, et al. 2010; Shea, et al. 2010; Tzertzinis, et al. 2010), loss of *ecr* in *C. elegans* is so far the only demonstrated case among ecdysozoans (Fig. 1A). *C. elegans* is also known to lack any genes coding *usp* (Schumann, et al. 2018; Taubenheim, et al. 2021), and molting of *C. elegans* must be therefore independent of ecdysone (Chitwood and Feldlaufer 1990; Frand, et al. 2005; Hill, et al. 2013). Rather, the molting of *C. elegans* is regulated by a mechanism similar to the biological/circadian clock (Fig. 1C) (Hendriks, et al. 2014; Meeuse, et al. 2020; Tsiairis

77 and Großhans 2021; Meeuse, et al. 2023). For example, evolutionary conserved
78 components of circadian clock, HR3/NHR-23 (ROR), LIN-42 (Period), and KIN-20
79 (CK1ε/δ) dominantly regulate the molting periods in *C. elegans* (Kostrouchova, et al. 1998,
80 2001; Banerjee, et al. 2005; Frand, et al. 2005; Kouns, et al. 2011; Monsalve, et al. 2011;
81 Rhodehouse, et al. 2018; Patel, et al. 2022; Johnson, et al. 2023; Kinney, et al. 2023; Hiroki
82 and Yoshitane 2024; Lamberti, et al. 2024; Spangler, et al. 2024). Another circadian clock
83 component, E75/NHR-85 (Rev-Erb), is also known to be involved in the molting clock of
84 *C. elegans*; the temporal formation of HR3/NHR-23 and E75/NHR-85 heterodimer
85 generates a transcriptional pulse of the microRNA *lin-4* (Kinney, et al. 2023). Feedback
86 loops involving HR3/NHR-23 and other genes/microRNAs (e.g., *let-7*) have also been
87 identified in *C. elegans* (Kouns, et al. 2011; Patel, et al. 2022; Johnson, et al. 2023). NHR-
88 25, an ortholog of FTZ-F1 which regulates insect molting, is a regulator of *C. elegans*
89 molting, while its function is likely minor as through miRNA expression control (Fig. 1B,
90 C) (Gissendanner, et al. 2004; Hayes, et al. 2006; Hada, et al. 2010; Meeuse, et al. 2023).
91 Other transcription factors such as GRH-1 have been also identified as a molting regulator
92 in *C. elegans* (Fig 1C) (Hauser, et al. 2022; Meeuse, et al. 2023).

93 Molting regulation of *C. elegans* is likely a derived state within nematodes. The
94 loss of *ecr in C. elegans* is also inconsistent with the idea that molting regulation is
95 conservative and stereotypic in nematodes, in which most species consistently molt four
96 times regardless of the divergence in the life cycles (Malakhov 1986). Thus, it is generally
97 considered that the loss of *ecr* in nematodes is a specific and rare event unique to *C. elegans*
98 (Taubenheim, et al. 2021), and elucidating the evolutionary background of *ecr* loss has
99 been a long-standing challenge. The loss of *ecr* in *C. elegans* is a critical subject for
100 understanding the evolution of ecdysozoan molting since it is implied that the key regulator
101 for molting can be altered during evolutionary processes. In summary, the case of *C.*
102 *elegans* raises doubts on the evolutionary conserved role of ecdysone.

103 This study investigated the evolutionary trajectory leading to the loss of *ecr* and *usp*
104 in nematodes, aiming to elucidate how key regulators of ecdysozoan molting can be altered.
105 We examined the presence of *ecr* and *usp* in a total of 160 nematode species and elucidated

106 the evolution of nematode molting regulation using genomic, transcriptomic, and protein
107 prediction analyses.

Results

1. Multiple losses of *ecr* and *usp* genes in Rhabditina and Tylenchina nematodes

Although *ecr* genes have been identified in some nematodes outside *Caenorhabditis* (Fig. 1A) (Shea, et al. 2004; Graham, et al. 2010; Parihar, et al. 2010; Shea, et al. 2010; Tzertzinis, et al. 2010), the specificity of *ecr* loss has been insufficiently explored within a phylogenetic framework (Fig. 1A). Thus, using publicly available genomic and transcriptome data, we searched for *ecr* across 160 nematode species including major nematode taxa (Fig. 2A, B, 159 genomic and 1 transcriptomic data, see also the methods). The genes of *ecr* were searched using BLAST and phylogenetic analysis (see the methods).

Gene mining of ecr and usp in 160 nematode species

Our search identified *ecr* genes from all major nematode taxa, including the sister group of all remaining nematodes, Enoplida (Fig. 2A). In Rhabditina, *ecr* was not found in any *Caenorhabditis* species examined (Fig. 2A), and the loss of *ecr* is specific to this lineage. Unexpectedly, *ecr* is also absent in 26 of 41 Tylenchina species examined (Fig. 2A). No *ecr* was found in the species of Tylenchomorpha, Strongyloididae, and Alloionematidae, and the latest phylogenic analyses consistently support the polyphyly of the three groups (Fig. 2C, see methods) (Smythe, et al. 2019; Ahmed, et al. 2022; Qing, et al. 2024). Thus, the loss of *ecr* is indicated as occurring twice in Tylenchina (Fig. 2A, C). We also mapped the presence and absence of *ecr* onto the phylogenetic trees reconstructed by Ahmed et al., 2022, and the occurrence of multiple losses of *ecr* is still supported (Fig. S1). Together, the loss of *ecr* occurred at least three times during nematode evolution. Note that the *ecr* genes, previously identified in *Strongyloides* species (Gonzalez Akimori, et al. 2021), are incorrectly annotated (Fig. S2).

C. elegans is also known to lack the gene encoding USP (Taubenheim, et al. 2021), a typical heterodimer partner of ECR. Our gene mining revealed that *usp* is also absent in several lineages of Rhabditina and Tylenchina (Fig. 2A). Especially, the loss of *usp* is detected not only in the species lacking *ecr* but more broadly observed as no *usp* was

137 identified in some Rhabditina species having *ecr* (ex., Strongylida: Fig. 2A, C). The loss
138 of *usp* also precedes the loss of *ecr* in Tylenchina as only Steinernematidae have both *ecr*
139 and *usp* (Figs 2A, C, and S1). Thus, it is suggested that the ECR-USP functionality has
140 been lost several times in nematodes. Interestingly, *ecr* was lost only in the lineages which
141 lost *usp* among the species examined, and *ecr* and *usp* losses are not related to specific
142 lifestyle/habitat (Fig. 2A).

143

144 *Additional analyses of ecr and usp loss*

145 We confirmed that the absence of *ecr* and *usp* is not due to technical errors or low-quality
146 genome assembly (Figs S3–S5, genome size, number of scaffolds, assembly N50, and
147 BUSCO score). As these figures show, no association with specific metrics was observed.

148 We also surveyed ecdysone receptors (*ecr* and *usp*) and biogenetic genes
149 (Halloween genes, Fig. 1B) in ecdysozoans and nematodes, respectively, motivated by our
150 unexpected finding of multiple *ecr* losses. We obtained consistent results with previous
151 reports. For example, *ecr* was newly identified in all ecdysozoan species examined (Fig.
152 S6): nematomorphs (Gordioida and Nectonematoida), tardigrades (Heterotardigrada),
153 kinorhynchs, and priapulids. No Halloween genes (*spo*, *phm*, *dib*, *sad*, or *shade*) were
154 identified in any of the nematode species examined.

155

156 **2. Putative modification of ecdysone hormone's roles in molting regulation with the**
157 **loss of *ecr* and *usp* genes**

158 We subsequently examined the evolutionary background of multiple losses of *ecr* and *usp*.
159 We first speculated that the involvement of ecdysone in molting regulation is specifically
160 lost in parallel with *ecr* and *usp* losses. To test this hypothesis, we performed the following
161 pharmacological functional and temporal gene expression analysis.

162

163 *ECR antagonist suppresses the molting process of Plectida nematodes which possess ecr*
164 *and usp genes*

165 To investigate the function of ecdysone hormone in nematode molting, we examined the
166 effects of the ECR antagonist, Cucurbitacin B (CucB), treatment on the molting of three
167 nematode species (Fig. 3A): *C. elegans* (Rhabditina lacking *ecr* and *usp*), *Diploscapter*
168 *pachys* (Rhabditina lacking *usp*), and *Plectus sambesii* (Plectida having *ecr* and *usp*). The
169 phylogeny of the three species reflects the evolutionary changes of *ecr* and *usp* losses (Fig.
170 3A, B).

171 In all species examined, larval worms molted four times after hatching to become
172 gravid adults (L1–L4 and adult stages). We collected synchronized L1 larvae and
173 monitored growth speed and molting timing after feeding for each species on optimized
174 agar culture plates at 20 °C (see Methods, Fig. S7A). Gonadal development was primarily
175 used as the key for defining specific larval and adult stages (Fig. S7B, C) (Tahseen, et al.
176 1991; TAHsEEN, et al. 1992; Hubbard and Greenstein 2000; Schindler and Sherwood
177 2013). For example, elongated gonadal primordia were observed after the L3 stage, and
178 the vulva developed clearly only after the L4 stage (Fig. S7B, C) (Hubbard and Greenstein
179 2000). Regarding molting cycle duration, *C. elegans* develops very rapidly, with young
180 adults emerging as early as two days after feeding at 20 °C (Figs. 3C, S7A). Growth in *D.*
181 *pachy* is slightly slower, requiring approximately three to four days after feeding until the
182 young adults emerge (Figs. 3C, S7A). *P. sambesii* is the slowest developer and molts
183 approximately every one to two days (Figs. 3C, S7A). Under our stable cultivation
184 conditions, larval growth was comparatively synchronous within each species.

185 We designed the CucB treatment experiments to target specific molting stages, as
186 shown in Figs 3C and S7A. For example, in *C. elegans* and *D. pachys*, CucB was applied
187 for two days, and we assessed whether treated worms progressed to the L4/adult and L3
188 stages, respectively (Fig. 3C). Feeding started with the treatment of CucB, and DMSO was
189 used as control. In *P. sambesii*, we performed two experiments (Fig. S7A). First, L1 worms
190 (0 days after feeding) were treated with CucB for three days, and their development to the
191 L2 stage was examined at the day three (Fig. 3C). Second, we targeted the progression
192 from L3 to L4 by applying CucB for three days starting at day 4 after feeding (Fig. S7A).
193 Based on preliminary toxicity assays, a concentration of 50 μM CucB was used
194 consistently in all experiments (three replicates).

195 Results are shown in Figs 3D–X, S8 and Table S2, and the effects on molting were
196 only observed in *P. sambesii*. Around 80% L1 worms developed to L2 worms in the control
197 experiments (DMSO, 24 of 29 worms, Fig. 3Q–S, W), while only around 20% worms
198 molted to L2 in CucB treatment (7 of 32 worms, Fig. 3T–V, W). In the remaining 25 of 32
199 CucB-treated L1 worms, apolysis process (a first step of molting process) occurred around
200 mouth parts (Fig. 3T–U), but their development/growth was arrested at this stage. Some
201 worms also molted the tail parts but did not complete molting process (Fig. 3V). Such
202 phenotypes are considered as molting defects or growth arrest at molting stage. Although
203 molting arrest was observed in some control worms (7/32, Fig. 3X), the difference between
204 two treatments was statistically significant (p=0.0032, Two Sample t-test, Fig. 3X). We
205 also observed similar phenotypic effects of CucB treatment in the experiments targeting
206 L3-L4 molting (growth: 39/45 [DMSO], 8/58 [CucB]; molting arrest: 0/45 [DMSO], 49/58
207 [CucB]; Fig. S8). These effects of CucB on molting resemble the observations in the
208 examples of insects and tardigrades (Toyofuku, et al. 2021; Yamakawa and Hejnol 2024).
209 Especially, considering that the CucB-treated worms proceed to apolysis stage, CucB is
210 suggested to specifically suppress the ecdysis process.

211 On the other hand, no effects on growth and molting were observed in *C. elegans*
212 (Fig. 3E–J). Almost all worms developed to L4/adult stages (DMSO: 55/58, CucB: 48/50)
213 and no molting defects were found (Fig. 3I, J). This result is consistent with the ecdysone-
214 independent molting in *C. elegans*. Interestingly, CucB treatment did not affect the growth
215 and molting of *D. pachys* which has *ecr* genes but not *usp* (Fig. 3K–P). Of 49 L1 worms,
216 47 and 46 worms grew to L3 stage in DMSO and CucB, respectively (Fig. 3O), and molting
217 arrest was found in only two CucB treated worms (Fig. 3P). Since we used the same
218 concentration of CucB among the three species, its effects may be more severe in smaller
219 bodied worms. Nevertheless, molting was unaffected by CucB in *D. pachys*, the smallest
220 of the three examined species, at a concentration sufficient to suppress molting in the larger
221 species, *P. sambesii* (Fig. 3B).

222

223 *Conserved temporal expression of ecr and usp during molting cycle in Trichinellida,*
224 *Spirurina, and Rhabditina nematodes*

225 We next examined the temporal expression patterns of *ecr* and *usp* in the representative
226 nematodes. Previous studies have shown that molting-related genes, including *ecr*, exhibit
227 oscillatory expression peaking just before ecdysis in various ecdysozoan species (Gao, et
228 al. 2015; Liu, et al. 2022; Yamakawa and Hejnol 2024). Based on this, we investigated if
229 the temporal expression of *ecr* and *usp* shows similar pattern during molting cycle among
230 nematode species.

231 We examined the temporal expression of *ecr* during the molting cycles of four
232 nematode species (Fig. 4A, B, Rhabditina: *Pristionchus pacificus* [having *ecr* and *usp*],
233 *Ancylostoma ceylanicum* [lacking *usp*], Spirurina: *Brugia malayi*, and Trichinellida:
234 *Trichuris suis*), for which transcriptome data during the molting cycle are publicly
235 available (see methods and Fig. S9). In *T. suis*, *ecr* expression showed a sharp peak pattern
236 before L3-L4 and L4-adult molting (Fig. 4B). Similar (but more moderate) peaked
237 expression was observed in L3-L4 molting of *B. malayi* (Fig. 4B). On the other hand,
238 although a pulsed expression of *ecr* was detected in L2-L3 and L3-L4 molting of *P.*
239 *pacificus*, the expression peaks did not precede the start of molting but peaked at the same
240 time (or later) as ecdysis, the final step of molting (Fig. 4B, see also the method and Fig.
241 S9). Importantly, the expression of *ecr* in *A. ceylanisum*, which lacks *usp*, showed a
242 comparatively minor increase during L3-L4 molting (Fig. 4B).

243 We also investigated the expression of *usp* genes in three species which possess *usp*
244 (Fig. 4A, C: *P. pacificus*, *T. suis*, and *B. malayi*). Similar to *ecr*, *usp* also shows a peaked
245 expression pattern before molting in *T. suis* and *B. malayi* (Fig. 4B). The temporal
246 expression of *ecr* and *usp* is similar in both species (Fig. 4B–D). *usp* of *P. pacificus* also
247 shows comparatively similar expression pattern with *ecr* (Fig. 4B–D), although the
248 expression pattern is less clearly overlapped than in *T. suis* and *B. malayi* (Fig. 4B–D).
249 Similar expression of *P. pacifucs ecr* and *usp* was previously observed during molting
250 cycles in a semi-quantitative PCR analysis (*Ppa-pnhr2* and *Ppa-pnhr-1*, respectively, 3–
251 48 hours after hatching with a three-hour interval) (Parihar, et al. 2010).

252

253 *Summary of pharmacological and expression analysis*

254 ECR antagonist suppresses the molting process of a Plectida species, and the peaked
255 expression of *ecr* and *usp* before molting is conserved in Trichinellida, Spirurina, and some
256 Rhabditina nematodes (e.g., *P. pacificus*). They all possess both *ecr* and *usp* genes.
257 Pharmacological suppression of ECR has been also reported to inhibit the molting process
258 in the Spirurina species *Dirofilaria immitis* (Warbrick, et al. 1993). However, such molting
259 suppression and peaked expression of *ecr* are not observed in the species lacking *ecr* and/or
260 *usp*. Thus, it is plausible to interpret that involvement of ecdysone/*ecr* in molting process
261 is altered and even lost in parallel with the loss of *ecr* and *usp* in the Plectida+Rhabditida
262 (Rhabditina, Tylenchina, and Spirurina) taxon.

263

264 **3. Screening for conserved molting regulators among nematodes**

265 Although we found the putatively divergent molting function of ECR, the molting process
266 itself appears consistent across nematodes (e.g., most nematodes consistently molt four
267 times (Malakhov 1986)). This suggests the presence of other key regulators which buffer
268 the loss of *ecr* and *usp*. As a first step toward identifying potential candidate genes, this
269 study focused on the *C. elegans* molting regulatory genes (Fig. 1C). Specifically, we
270 examined the expression pattern of the five representative regulators (Fig. 1C): *hr3* (*nhr-*
271 *23*), *lin-42* (*per*), *kin-20 (ck1/ ε δ)*, *e75* (*nhr-85*), and *ftz-f1* (*nhr-25*).

272 First, our survey revealed that all genes are highly conserved across nematode
273 lineages (Fig. 2A). Only *e75* genes may be lost in some *Pristionchus* and *Panagrolaimus*
274 lineages (Fig. 2A). We then examined the expression pattern of the five genes during the
275 molting cycle in six nematode species (Fig. 5, the above four species, *ecr*-lacking
276 Rhabditina *C. elegans*, and *ecr*-lacking Tylenchina *Globodera pallida*). Notably, pulsed
277 expression of *hr3* prior to molting was observed in all six species (Fig. 5B). For example,
278 *hr3* expression shows a peaked pattern prior to molting in *A. ceylanisum* which does not
279 show peaked *ecr* expression, and *G. pallida* which lacks *ecr* (Figs 4B, 5B). A similar
280 expression pattern was observed in *lin-42* of *C. elegans*, *A. ceylanicum*, *P. pacificus*, and

281 *B. malayi* (Fig. 5C). However, this pattern was not observed during the molting process of
282 *G. pallida* and *T. suis* (Fig. 5C). The temporal expression patterns of *kin-20*, *e75* and *ftz-f1*
283 are also not conserved among the six species examined (Fig. 5D–F).

284 We also performed systematic and unbiased screening of the candidate conserved
285 molting regulators across the above six species. Previously, the genes showing oscillatory
286 expression during the molting cycle were extracted from *C. elegans* (1,592 genes) and *P.*
287 *pacificus* (2,964 genes) (Kim, et al. 2013; Sun, et al. 2021). For the remaining four species,
288 we performed a fuzzy c-mean clustering analysis on each transcriptome dataset and
289 extracted the cluster(s) showing peaked expression just before molting in each species (Fig.
290 S10; green shades; *A. ceylanicum*: 8,110; *G. pallida*: 3,383; *B. malayi*: 7,114; and *T. suis*:
291 2,896 genes). Then, we used OrthoFinder to extract orthologous groups (OGs) among the
292 screened genes (Emms and Kelly 2019). Of the total 5,180 OGs identified, we found that
293 55 OGs contain one or more genes from all species. For example, a total of 168 *C. elegans*
294 genes were assigned to any of the 55 OGs (Table S2). Genes involved in cuticle
295 development were included in the 55 OGs (e.g., nematode cuticle collagen [col-125, col-
296 33, col-133/OG0000005]), supporting the feasibility of detecting molting-related genes.
297 Finally, we searched for transcription factor genes among 168 *C. elegans* genes, based on
298 their domain structure. We found that only three OGs include transcription factor genes.
299 Notably, although molting regulatory functions have not been reported in two OGs
300 (OG0000071/Homeobox: *lin-39* and *nob-1*; OG0000130/zf-C2H2: *sptf-2* and *znf-782*), our
301 screening results included *hr3* (OG0000063/Hormone_receptor, zf-C4). No other nuclear
302 receptor genes were identified as candidate genes from this screening. Note that some
303 transcription factors, such as *grh-1* and *blmp-1*, which are involved in the molting
304 regulation of *C. elegans* (Meeuse et al., 2023), were not extracted in this screening (Fig.
305 S11). For example, the peak expression of both genes before molting is comparatively
306 conserved among the examined species; this pattern was not observed, or expression was
307 only observed very weakly in *G. pallida* (Fig. S11).

308 In conclusion, our targeted approach and unbiased screening both detected *hr3/nhr-*
309 *23* as a potent candidate conserved regulator of nematode molting. This gene potentially
310 buffers the loss of multiple ECR genes and their functions.

311

312 **4. Extensive expansion of nuclear receptors and their structural diversification in**
313 **Rhabditina and Tylenchina**

314 In order to understand the evolutionary background that *ecr* and *usp* genes are specifically
315 lost within Rhabditina and Tylenchina among nematodes, we focused on that Rhabditina
316 and Tylenchina extensively expanded nuclear receptor (NR) genes (Sural and Hobert
317 2021). The following analyses tested the hypothesis that the expansion of NR contributes
318 to the specific losses of ECR and USP among nematodes.

319

320 *Stepwise expansion of nematode NRs*

321 We first reconstructed the evolutionary process of NR expansion. NRs were identified by
322 extracting proteins with NR conserved domains from 160 nematode species. Plotting the
323 number of NRs in the phylogenetic tree shows that NR expansion proceeded in a stepwise
324 manner under phylogenetic constraints (Fig. 6A). We then extracted orthogroups (OGs) of
325 NRs from represented 11 species (1–3 species from each Rhabditina, Tylenchina,
326 Spirurina, Trichinellida, and Enoplida; Figs 6, S12). This analysis showed that the common
327 ancestor of nematodes has at least 12 OGs, and NRs increased to 34 OGs in the ancestor
328 of Rhabditida (Figs 6A, B, S12: Spirurina/Rhabditina/Tylenchina). Finally, the ancestor of
329 Rhabditina/Tylenchina acquired additional 22 OGs (total 56 OGs), and Rhabditina and
330 Tylenchina ancestrally had 136 and 75 OGs, respectively (Figs 6A, B, S12). Some
331 nematodes such as *Plectus sambesii* also increased NRs (Fig. 6A), while *ecr* and *usp* are
332 not missing. Thus, although expansions of NRs was not strictly associated with the loss of
333 *ecr* and *usp* in some lineages, it is still important to point out that Rhabditina and
334 Tylenchina are unique to have abundant NRs among nematodes.

335

336 *Structural divergence of expanded HNF4 proteins in nematodes*

337 Since HNF4 subtype genes are specifically expanded in nematodes among various NR
338 genes (Bonneton, et al. 2008; Kostrouchova and Kostrouch 2015), it is unclear if such

339 HNF4 proteins contributed to the loss of different NR subtype proteins, ECR and USP. We
340 assumed that the expanded HNF4 proteins diverged in structural functionality and
341 convergently evolved a similar feature with ECR and USP. In order to test this hypothesis,
342 we compared the structural features of ligand-binding domain (LBD), a core domain of
343 NRs that interact with ligands and other proteins, between nematode "ancestral" and
344 "expanded" HNF4s.

345 Nematodes ancestrally have a single HNF4 protein, and those proteins are
346 conserved in early-branching taxa, such as Enoplida, Trichinnelida, and Monhynelida (Fig
347 2A, B). We predicted the protein structure of HNF4 LBD from 20 species of those groups
348 using Colabfold/Alphafold2 (see the Methods). To investigate whether "ancestral" HNF4-
349 LBDs have conserved HNF4-specific features, we compared each of the 20 predicted
350 protein models with each NR LBD of the model insect *D. melanogaster* using TM-align
351 (16 NRs, see also the Methods). The TM-score of each pairwise comparison was visualized
352 as a heatmap in Fig. 7A. Highly specific and conserved LBD structural similarity is found
353 between the nematode "ancestral" HNF4 and *D. melanogaster* HNF4 (Fig. 7A, B).
354 Although some nematode HNF4s also show a comparatively high score with nonHNF4
355 NRs (Figs 7A, S13A), the TM-score from the comparison with *D. melanogaster* HNF4 is
356 the highest among all species examined (Fig. S13B, C).

357 We conducted the same analysis on "expanded" HNF4s from Rhabditina and
358 Tylenchina species. In this analysis, we predicted the structure of 260 and 60 HNF4 LBD
359 which were extracted from *ecr*/*usp*-lacking Rhabditina *C. elegans* and Tylenchina
360 *Meloidgyne Ingonita*, respectively (see also the Methods for the details). Unlike "ancestral"
361 HNF4 proteins, more than 80% of examined proteins in both species do not necessarily
362 show the highest TM-score with HNF4 among *D. melanogaster* 16 NRs (Fig. 7A,
363 B).Notably, 52 (20%) and 85 (32.7%) proteins from *C. elegans* shows the highest TM-
364 scores with ECR and USP, respectively (Fig. S13B). Similar results were also found in *M.*
365 *Ingonita* (15 [25%] and 25 [41.6%], respectively, Fig. S13B). This analysis suggests the
366 divergence of structural features of HNF4 LBDs during nematode NR expansion.

367

368 *A case study finding nematode HNF4s which evolve a novel heterodimer functionality with*
369 *ECR*

370 The above analysis implied that some HNF4 proteins acquire new structural features during
371 expansion events in Rhabditina and Tylenchina. To further test whether some HNF4
372 proteins evolved to functions equivalent to ECR or USP, we performed a case study to
373 screen HNF4s which evolved USP-like functions in nematodes.

374 First, we searched for NRs with a structural feature similar to USP in the model
375 nematode *C. elegans* using the Foldseek search tool (van Kempen, et al. 2024). The LBDs
376 of ECR and USP have been experimentally determined to form a heterodimer (Hill, et al.
377 2013; Browning, et al. 2021). Thus, using the LBD of the USP protein from *D.*
378 *melanogaster* as the query, we searched the AFDB-proteome database of *C. elegans*
379 (UP000001940). As a result, we identified five candidate NRs with the top hit score (Table
380 S3: NHR-64, NHR-69, NHR-35, NHR-14, and NHR-49). By investigating the presence of
381 these proteins in other nematode species, we confirmed that all five proteins evolved from
382 the HNF4 NR subtype within nematodes (=expanded HNF4s, Figs S14, S15F).

383 We used the ColabFold tool with AlphaFold2-Multimer to test if our target proteins
384 could form a heterodimer with ECR (Jumper, et al. 2021; Evans, et al. 2022; Mirdita, et al.
385 2022). First, we validated that the ECR-USP heterodimer structure is correctly predicted
386 in *D. melanogaster*. The predicted structural alignment of the ECR-USP heterodimer is
387 highly consistent with the experimentally determined ECR-USP heterodimer (Fig. 7C)
388 (Hill, et al. 2013; Browning, et al. 2021), and the ipTM (interface predicted template
389 modeling) score is greater than 0.9. Furthermore, the PAE (predicted alignment error)
390 heatmap clearly shows the high certainty of each ECR and USP prediction (Fig. 7D, second
391 and fourth quadrants [Fig. 7G]) as well as the interaction of ECR and USP (Fig. 7D, first
392 and third quadrants [Fig. 7G]). Conversely, a high-probability heterodimer interaction was
393 not predicted when testing ECR and HNF4, which heterodimer functions have not been
394 reported in *D. melanogaster* (Fig. 7E, F, ipTM = 0.15). The PAE heatmap shows that the
395 interface of ECR and HNF4 is not accurately predicted (Fig. 7F; high error ratio [red color]
396 in the first and third quadrants [Fig. 7G]), suggesting that the predicted alignment is likely

397 due to random coincidence (Evans, et al. 2022). Thus, we confirmed that this analysis
398 shows consistent results with the previous structural analysis.

399 We tested whether each candidate protein (NHR-64, NHR-69, NHR-35, NHR-14,
400 and NHR-49) forms a heterodimer with *D. melanogaster* ECR. As shown in the analysis
401 of ECR and HNF4 in *D. melanogaster*, heterodimer interaction was not clearly detected
402 for three of the five proteins (Fig. S15A–E: NHR-35, NHR-14, and NHR-49; piTM =
403 0.209, 0.68, and 0.166, respectively). Notably, however, our results clearly predicted that
404 NHR-64 and NHR-69 form a heterodimer with ECR (Fig. S15A, B, ipTM = 0.805 and
405 0.887, respectively). The structure of the putative heterodimer resembles that of the *D.*
406 *melanogaster* ECR-USP heterodimer (Figs 7C, S15A-B). We furthermore performed yeast
407 two-hybrid assay to validate the predicted heterodimer interaction of NHR-64 and NHR-
408 69 in *in vivo* system (Fig. S15G, H). We first validated that our assay detected a weak and
409 spontaneous interaction between ECR and USP without ligand in *D. melanogaster* (Fig.
410 S15H), as shown in the previous studies (Lezzi, et al. 2002; Bitra and Palli 2009). We then
411 investigated an interaction of *D. melanogaster* ECR and *C. elegans* NHR-64 or NHR-69
412 (Fig. S15H). Among the two proteins, interaction between *D. melanogaster* ECR and *C.*
413 *elegans* NHR-64 was observed in this experiment.

414 We found that not only *C. elegans* but other Rhabditina and Tylenchina nematodes
415 have orthologs of NHR-64 that exhibit similar structural features based on *in silico*
416 structural prediction (Fig. 7J: *Globodera pallida* NHR-64 [ipTM = 0.878]; Fig. 7K:
417 *Pristionchus pacificus* NHR-64 [ipTM = 0.705]; and Fig. S16B: Other examples). Our
418 analysis also predicted that *C. elegans* NHR-64 can form a heterodimer with ECR of the
419 nematode *Brugia malayi* (Fig. S16C). Moreover, we investigated the structural feature of
420 "ancestral" HNF4 proteins (Figs 7H, I, and S16A). Interestingly, such HNF4s were not
421 predicted to interact with ECR heterodimers (Fig. 7H: *Pontonema vulgare* [ipTM = 0.241];
422 Fig. 7I: *Trichuris muris* [ipTM = 0.181]; Fig. S16A: other examples). This is similar to the
423 results of the ECR-HNF4 comparison in *D. melanogaster* (Fig. 6C). Taken together, our
424 analyses suggests that some HNF4s evolved distinct structural features for dimerization
425 during the NRs/HNF4s expansion within nematodes.

426 **Discussion**

427 This study found that loss of *ecr* and *usp* is not unique to *Caenorhabditis* but has occurred
428 multiple times within nematodes. Here we discuss that molting regulation by an alternative
429 regulator and the expansion of NRs may explain the specific losses of *ecr* and *usp* within
430 Rhabditina and Tylenchina species.

431

432 *Evolutionary scenario of nematode molting regulation*

433 Based on the previous reports and our findings (ex., Figs 1, 3–4), it is implied that ecdysone
434 is ancestrally involved in the molting regulation of Rhabditida (a clade of Spirurina,
435 Rhabditina and Tylenchina) nematodes. Although it is still difficult to specify the
436 regulatory role of ecdysone hormone in nematode molting (see the discussion below),
437 involvement of ecdysone hormone plausibly changes in parallel with the losses of *ecr* and
438 *usp* within Rhabditina and Tylenchina. We hypothesize that three aspects underlie this
439 evolutionary process.

440 First, considering that molting of nematodes is consistent regardless of *ecr* and/or
441 *usp* losses, the presence of other key molting regulators is implied. This study showed that
442 HR3/NHR-23 is a potent candidate for the key regulator across nematode taxa. HR3/NHR-
443 23 plays a key regulatory role in *C. elegans* molting, and this function may be conserved
444 among a wide range of nematode taxa. Note that some components of *C. elegans* molting
445 regulation, such as Lin-42, also show a conserved expression pattern during molting cycle
446 among different nematodes (Fig. 5). This suggests that not only HR3 but also other genes
447 may be involved in the molting of nematode ancestors. With such regulatory machinery,
448 the loss of *ecr* and *usp* may be buffered without having catastrophic effects on the molting
449 process itself.

450 Second, we propose that the loss of *usp* is a critical step toward the loss of *ecr*. This
451 study revealed that *ecr* loss occurred only in lineages lacking *usp* (Fig. 2A). This may be
452 because the loss of USP likely led to the altered regulatory interaction and functionality of
453 ECR. Indeed, Graham et al., 2010 experimentally showed that ECR of *Haemonchus*
454 *contortus* (usp-lacking Rhabditina) cannot form heterodimers with the USP of the red louse

455 *Bovicola bovis*. Kostrouchova and Kostrouch 2015 also discussed changes of NR
456 heterodimer functionality along loss of USP in *C. elegans*. As shown in our findings on the
457 ECR-antagonist treatment and *ecr* expression in *usp*-lacking species (Figs 3, 4), the
458 function of *ecr* in molting regulation may become minor or lost with the loss of *usp*. This
459 is also consistent to that 20E treatment did not affect the L3-L4 molting of *H. contrtus*
460 (Graham, et al. 2010). Although this hypothesis serves an interesting insight that usp-
461 lacking species may represent an intermediate state of *ecr* loss, it is also important to note
462 that some species of *usp*-lacking Rhabditina, such as *H. contortus* and *Heligmosomoides*
463 *polygyrus*, are reported to exhibit endogenous ecdysone and pharmacological induction of
464 molting by ecdysone (Dennis 1976; Fleming 1993). A detailed analysis of molting
465 regulation in *usp*-lacking Rhabditina and Tylenchina is required for further assessing our
466 hypothesis.

467 Finally, it seems critical that HNF4 subtype genes, the same NR subfamily with
468 USP, have undergone extensive expansion in Rhabditina and Tylenchina (Bonneton, et al.
469 2008; Kostrouchova and Kostrouch 2015). This study suggests the divergence of the LBD
470 structure of expanded HNF4 in *C. elegans* and *M. incognita* (Fig. 7A, B). We also screened
471 a HNF4 protein which have a heterodimer functionality with ECR of *D. melanogaster* (Fig.
472 7C–M). These results are also consistent to the previous findings of the emergence of novel
473 heterodimer pairs within expanded HNF4s in *C. elegans* (e.g., NHR-80 and NHR-49)
474 (Pathare, et al. 2012). Based on these findings, it can be expected that expanded HNF4 can
475 take over the function of USP, which may lead to USP loss and change in NR functionality.
476 While this study did not address the causality of ECR loss, some HNF4 proteins may have
477 convergently evolved the ECR-like structures/functions. Although NHR-64 represents an
478 intriguing candidate for a representative protein which took over a USP-like function,
479 considering that involvement of *nhr-64* in molting regulation is unclear (Gissendanner, et
480 al. 2004; Liang, et al. 2010), further characterization of NHR-64 function and other
481 expanded HNF4s across nematode species is required. In any case, this study raises the
482 possibility that extensive NR expansion explains the specificity of *ecr*/*usp* losses among
483 nematodes.

484

485 *Evolutionary impacts of structural divergence of nematode expanded NRs*

486 The expansion of nematode NRs has been regarded as a "natural experiment made by a
487 phylum" (Kostrouchova and Kostrouch 2015), and its evolutionary significance has been
488 widely studied (Taubert, et al. 2011; Antebi 2015; Kostrouchova and Kostrouch 2015;
489 Sural and Hobert 2021). For example, Sural and Hobert (2021) proposed that the expansion
490 of NRs is associated with a free-living lifestyle. They reported that the expression of NRs,
491 GPCRs, and insulin genes is enriched in the sensory neurons of *C. elegans* (Sural and
492 Hobert 2021). Based on the findings, they hypothesizes that NRs may integrate sensory
493 and/or internal information (Sural and Hobert 2021). It has also been suggested that NRs
494 expanded in response to xenobiotics in free-living nematodes (Lindblom, et al. 2001;
495 Lindblom and Dodd 2006). Notably, various other functions have been reported in addition
496 to these examples (Taubert, et al. 2011; Antebi 2015; Kostrouchova and Kostrouch 2015).
497 In this study, we found that NR expansion proceeded in a stepwise manner under
498 phylogenetic constraints (Fig. 6) and that NRs evolved novel structural features (Fig. 7).
499 We would like to discuss that our findings are not contradictory to previous research. For
500 example, some parasitic lineages lost many NRs after the expansion of NRs in Rhabditina
501 (Fig. 6A), which supports the association between NR expansion and a free-living lifestyle
502 in this group. Additionally, our findings about changes in NR structural features shows
503 affinity with the divergence of NR functions. We propose that changes in NR functionality,
504 including heterodimeric potential, may be a driving force behind divergent NR functions
505 in nematodes. Further investigation into the causes and consequences of NR expansion in
506 nematode evolution is of great importance.

507

508 *Insights into evolution of nematode and ecdysozoan molting*

509 Further experimental assessment of the role of the ecdysone hormone in nematodes is
510 required for clarifying the evolutionary background of changes in the molting regulatory
511 machinery. For example, the regulatory roles of *ecr and usp* need to be tested at the level
512 of gene function in various nematodes. Recently, gene function assays have been

513 established in several non-model nematode species, such as *Auanema*, *Steinernema*, and
514 *Panagrolaimus* (Adams, et al. 2019; Cao 2023; Hellekes, et al. 2023). With this
515 methodological development, it is critical to test if ecdysone/ecr regulates all four molting
516 processes and it has a master regulatory role as seen in arthropods. Elucidating the
517 ecdysone biogenesis process is also necessary. In particular, since ecdysone synthesis in
518 nematodes is independent of Halloween genes (which are arthropod-specific P450 genes,
519 Fig. 1B, Schumann et al., 2018), screening the P450 gene family is essential to identifying
520 the genes responsible for ecdysteroid synthesis in nematodes. Finally, we note that
521 ecdysone hormone likely has pleiotropic functions, including those related to reproduction,
522 in nematodes. The relationship between such biological processes and the loss of ecr/usp
523 is an important subject for future study.

524 Apart from ecdysone hormone, it is interesting that temporal expression of *hr3/nhr-*
525 *23* during molting cycle is highly conserved among nematode species examined (Fig. 5B).
526 Based on this finding, we provide the hypothesis that HR3 plays a dominant role as an
527 ancestral and conserved molting regulator in nematodes and possibly even in ecdysozoans
528 (note that HR3 is also a core molting regulator in arthropods (Yamanaka, et al. 2013) and
529 putatively in tardigrades (Yamakawa and Hejnol 2024)). HR3 is also highly conserved
530 among ecdysozoan species (Fig. S6). Considering that HR3 orthologues ROR and NHR-
531 23 are known to be involved in regulation of circadian clocks among bilaterians (Patke, et
532 al. 2020; Hiroki and Yoshitane 2024; Patil and van Zon 2024), the ancestry of HR3 shows
533 an association with the origin of molting regulation, which control biological and
534 developmental time. It should be also noted that other circadian clock components such as
535 lin-42/per also shows a conserved temporal expression among different nematode species
536 (Fig. 5). Our results also provide the possible use of HR3 regulation of molting for medical
537 applications and pest control, in plant-parasitic and some human-parasitic nematodes,
538 which have lost ECR (Fig. 2A: Tylenchomorpha and Strongylida, respectively).

539

Materials and Methods

1. Data collection and target species

We obtained protein sequences of 159 nematode species from WormBase Parasite (version: WBPS19, WS291) (Howe, et al. 2017). These sequences/protein models were reconstructed from the genomic data. All accession numbers of the original dataset are available in the supplementary dataset. In this study, the gene ID was referenced to the original dataset, while also incorporating some modifications. For example, species identifiers were added to the beginning of the gene ID (i.e. *GeneID* → *NEMA_CaenoElega_GeneID*). Some characters, such as curly brackets, were also removed for later analysis. In addition, the transcriptome data of the Enoplida nematode *Pontonema vulgare* was obtained from NCBI (accession number: PRJNA504396). Quality of raw reads were examined using FastQC (version: v0.11.9; https://www.bioinformatics.babraham.ac.uk/projects/fastqc/). The subsequent filtering was performed using trimmomatic (version: 0.39) (Bolger, et al. 2014), and *de novo* assembly was conducted using Trinity (version: v2.13.2) (Henschel, et al. 2012). Transdecoder (version: 5.5.0; https://github.com/TransDecoder/TransDecoder) was used to obtain the peptide sequences of *P. vulgare* transcript models. The assembled sequences are available in the supplementary dataset.

The phylogenetic relationship of the target species was referenced to previous studies. For example, the topology of the major taxon phylogeny (grouped by color in Fig. 2) is consistent with three recent molecular phylogenetic reports (Smythe, et al. 2019; Ahmed, et al. 2022; Qing, et al. 2024). The relationship of Rhabditina and Tylenchina taxa is also consistent in the three reports (shown in Fig. 2C). Since the analysis by Ahmed et al. (2022) used the largest number of our target species, we modified their phylogenetic tree by adding our target species with referring to other literatures. If our target species were not included in their analysis, we referred to other literature. For example, we used Ahmed et al. (2022) to reconstruct the phylogeny of *Caenorhabditis* species, but the position of *C. auriculariae* was unclear in that study. In this case, we determined the position of *C. auriculariae* based on another study (Dayi, et al. 2021). The phylogenetic

569 positions of the following species were determined not only with reference to Ahmed et
570 al., 2022: *Angiostrongylus cantonensis* (Dumidae, et al. 2023), *Cylicocylus radiatus* (Hu,
571 et al. 2020), *Meloidogyne chitwoodi* (Álvarez-Ortega, et al. 2019), *Steinernema*
572 *hermaphroditum* (Schwarz, et al. 2025), *Aphelenchoides* species (Lai, et al. 2022),
573 *Cercopithifilaria johnstoni* (McCann, et al. 2021), and Enoplida species (Qing, et al. 2024).
574 The phylogeny of the two species, *Parelaphostrongylus tenuis* and *Bradynema listronoti*,
575 was unclear. Their phylogenetic positions were estimated by identifying their respective
576 family, Metastrongylidae and Allantonematidae, from the NCBI Taxonomy database
577 (https://www.ncbi.nlm.nih.gov/taxonomy). A Newick file for visualizing the phylogenetic
578 tree is available in the supplementary dataset. We also used the trees which were
579 reconstructed by Ahmed et al., 2022 to test the multiple losses of *ecr* and *usp* in Rhabditina
580 and Tylenchina. These files are available in the supplementary data of Ahmed et al., 2022,
581 which was uploaded in Figshare (https://figshare.com/s/946b2bc6aef7ce4a9e6a,
582 3_TYLENCHINA and 4_RHABDITINA).

583

584 **2. Gene identification**

585 *Screening*

586 Gene mining of *ecr*, *usp, hr3, e75, ftz-f1*, *lin-42*, and *kin-20* was conducted based on the
587 sequence similarity by combination of BLAST search and phylogenetic analysis with the
588 following screening. All sequences and phylogenetic trees are available in the
589 supplementary datasets.

590 We first performed a BLAST search using the query sequences of ECR, USP, HR3,
591 E75, and FTZ-F1 from *Drosophila melanogaster* against the database of each nematode
592 species. The query sequences are from UniProt (ECR: P34021, USP: P20153, HR3:
593 P31396, E75: P17672, and FTZ-F1: P33244). The peptides showing the hit with less than
594 1E-20 e-value were extracted and used as query sequences for the second BLAST against
595 the *D. melanogaster* database. This database was built using the CDS sequences from
596 FlyBase (dmel-all-CDS-r6.45.fasta) (Öztürk-Çolak, et al. 2024). For the screening of LIN-

597 42 and KIN-20, we used the query sequence and the database from *Caenorhabditis elegans*
598 (UniProt id: Q65ZG8 and Q20471, respectively). Finally, the peptides showing the
599 reciprocal top hit with less than 1E-10 e-value were extracted. Each candidate gene set of
600 ECR, USP, HR3, E75, and FTZ-F1 (181, 256, 342, 196, and 199 peptides, respectively)
601 was aligned with other known nuclear receptors (NRs) from different animals (the
602 sequences were previously used to identify NR genes (Vogeler, et al. 2014; Yamakawa and
603 Hejnol 2024) (see also the supplementary dataset) using MAFFT (version: v7.526, --auto
604 option) (Katoh and Standley 2013), and the alignments were filtered using trimAl (version:
605 1.4.1, threshold: 0.8) (Capella-Gutiérrez, et al. 2009). Candidate 203 proteins of LIN-42
606 were also aligned with other known Period, Clock, Arnt, and Bmal proteins using the same
607 methods (the sequences are available in the supplementary dataset). Candidate 303 proteins
608 of KIN-20 were aligned with KIN-19 and CSNK-1 proteins. Phylogenetic analysis of each
609 data set was performed using RAxML (version: 8.2.12, bootstrap: 1,000 generations,
610 raxmlHPC-PTHREADS-SSE3 -f a -x 12345 -p 12345 -# 1000 -m PROTGAMMAAUTO
611 —-auto-prot=aic -s *input_file* -n *output_file*) (Stamatakis 2014). Gene identity was
612 determined by examining, whether the candidate genes were included in the clade of target
613 genes with high bootstrap values. By removing the genes that did not belong to the target
614 clade, we finally identified 128, 74, 276, 151, 199, 132, and 220 peptide models as ECR,
615 USP, HR3, E75, FTZ-F1, LIN-42, and KIN-20 respectively (see the trees in the
616 supplementary dataset). Note that some species have multiple copies.

617 Next, the above identified target peptides were used as query sequences, and a
618 BLAST search was performed against the database of each nematode species in which the
619 target genes were not found in the first screening. Top-hit sequences with less than 1E-20
620 e-values were collected, and each sequence was used as a query for the second BLAST
621 search against the database of the original species from which the first query originated.
622 Then, genes showing the reciprocal one-to-one top-hit were finally accumulated as
623 candidates (ECR: 197, USP: 277, HR3: 28, E75: 77, FTZ-F1: 95, LIN-42: 151, and KIN-
624 20: 2 peptides). After selecting the peptides having DNA binding domain of NRs (except
625 LIN-42 and KIN-20, HMMER domain search [version 3.4] (Johnson, et al. 2010), see the
626 below for the details) and manually checking the accuracy of the gene domain (e.g., NCBI

627 conserved domain search: https://www.ncbi.nlm.nih.gov/Structure/cdd/wrpsb.cgi), we
628 finally investigated the identity of the selected peptides by phylogenetic analysis as
629 mentioned above. In this analysis, 5, 21, 1, 16, 28, ,17 and 0 peptide(s) were additionally
630 identified as ECR, USP, HR3, E75, FTZ-F1, LIN-42, and KIN-20, respectively. Finally,
631 the peptides obtained in the 2nd screening were used for the BLAST query sequences, and
632 we repeated the BLAST analysis as performed in the 2nd screening. However, no genes
633 were newly identified as ECR, USP, HR3, FTZ-F1, and LIN-42. Only 4 peptides were
634 additionally identified as E75.

635 Target genes were also searched by BLAST, Hmmer domain search (screening of
636 the genes having DNA or ligand binding domain of NRs, see also the below), and
637 phylogenetic analysis. For example, the BLAST search was performed with a higher e-
638 value threshold (ex. 1E-05). Different database was also explored for the species missing
639 the target genes, and ECR of *Steinernema feltiae* was identified using the other dataset in
640 WormBase Parasite (version: WBPS19, WS291) from the one which we originally used
641 (accession number: PRJNA204661). Finally, eight additional genes (nine peptides) were
642 identified to compensate for the missing target genes, and the results are summarized in
643 Fig. 2. Note that no *ecr* and *usp* genes were identified in the tblastn-based search on the
644 genome assembly of the species lacking these genes.

645

646 *Criteria for the presence and absence of target genes*

647 The summary of the screening and gene identification of 160 species is shown in Fig. 2A.
648 In some species, the target genes were missing even though the genes were found in species
649 of the same genus (or closely related species). Since this study avoided to distinguish
650 between species-specific loss and technical errors such as low data quality, gene missing
651 in these species were considered as missing information in Fig. 2A (question marks in Fig.
652 2A). We considered the loss to be reliable if the loss of the genes was observed in all the
653 same genus and closely related species. According to these criteria, we detected loss of *ecr*
654 only in *Caenorhabditis*, Tylenchomorpha, Strongyloididae and Alloionematidae (Fig. 2A).

655 Loss of *usp* was also reliable in Strongylida, Anarhabditis, non-Steinernematidae
656 Tylenchina (Fig. 2A).

657

658 *Gene identification in other ecdysozoans*

659 Previous works identified *ecr*, *usp* and *hr3* in insects (*Drosophila melanogaster*,
660 *Drosophila pseudoobscura*, *Anopheles gambiae*, *Aedes aegypti*, *Bombyx mori*, *Tribolium*
661 *castaneum*, and *Apis mellifera*), other arthropods (Myriapoda: *Strigamia maritima*;
662 Chelicerata: *Limulus polyphemus* and *Stegodyphus mimosarum*; and Branchiopoda:
663 *Daphnia pulex* and *Daphnia magna*), tardigrades (*Ramazzottius varieornatus* and
664 *Hypsibius exemplaris*), onychophorans (*Euperipatoides rowelli*), nematodes (*Brugia*
665 *malayi*, *Caenorhabditis elegans* [only *hr3*]), and priapulids (*Priaplus caudutus*) (Bonneton,
666 et al. 2008; Schumann, et al. 2018). In addition, we newly identified *ecr*, *usp*, and *hr3* in
667 tardigrades (*Echiniscus testudo*), nematomorphs (*Acutogordius australiensis*, *Gordionus*
668 *montsenyensis*, *Nectonema munidae*, *Paragordius varius*), kinorhynchs (*Campyloderes*
669 *vanhoeffeni*, *Franciscidere kalenesos*, *Dracoderes abei*) and priapulids (*Tubiluchus*
670 *corallicola*). For gene identification, we collected genomic or transcriptomic data from
671 publications or public databases (*E. testudo*: Murai et al., 2021 (Murai, et al. 2021), *A.*
672 *australiensis* and *N. munidae*: Cunha et al., 2023 (Cunha, et al. 2023) [FigShare:
673 doi.org/10.6084/m9.figshare.23419922], *G. montsenyensis*: Eleftheriadi et al., 2024
674 (Eleftheriadi, et al. 2024), *P. varius*: ERR1817116, ERR1817117, ERR1817118, and
675 ERR1817119 [NCBI SRA]; kinorhynchs: Herranz et al., 2022 (Herranz, et al. 2022) [*C.*
676 *vanhoeffeni*: SRR14509480, *F. kalenesos*: SRR14509483, and *D. abei*: SRR14509486]).
677 Raw read data from *P. varius* and kinorhynch species were *de novo* assembled as described
678 above. Gene identity was confirmed by BLAST and phylogenetic analysis using the same
679 methods as above. The results are summarized in Fig. S6, and the gene tree and sequences
680 are available in the supplemental dataset.

681

682 *Reannotation of the* ecr *genes identified by Gonzalez Akimori et al., 2021*

683 The seven ECR-1 genes used to identify ECR-1 of *Strongyloides stercoralis* in Gonzalez
684 Akimori et al. 2021 were obtained from NCBI GenBank (Gonzalez Akimori, et al. 2021).
685 The sequence of ECR-1 of *S. stercoralis* was not available due to unknown accession
686 number after their gene name modification (Gonzalez Akimori, et al. 2021). Phylogenetic
687 analysis was performed as described above, and the results are summarized in Fig. S2. We
688 also included the sequences of the ecdysozoan THR (Thyroid hormone receptor) genes
689 after preliminary test using the above dataset. All sequences for the tree are available in the
690 supplemental dataset.

691

692 *Genome assembly quality*

693 We obtained the quality metrics information for the genome assembly used in this study
694 from WormBase Parasite (version WBPS19, WS291) (Howe, et al. 2017). These metrics
695 include genome size, N50, scaffold number, BUSCO annotation score, and BUSCO
696 assembly score. These metrics are summarized in the phylogenetic trees in Figs S3–S5.

697

698 **3. Extraction of NRs and transcription factors based on the domain conservation**

699 The HMM profile of NRs (Hormone_recep: PF00104) was obtained from the Pfam
700 database. Using this profile as a query, hmmscan was performed against all peptide data of
701 the target species (threshold 1E-05) (Johnson, et al. 2010), and the identified genes were
702 considered as NRs. The number of genes was counted considering the isoforms and shown
703 in the linear bar graph of Fig. 5. We also used previously generated HMM profiles to screen
704 transcription factors (Yamakawa, et al. 2023). Shortly, the profiles include the following
705 targets: ARID (PF01388.17), AT_hook (PF02178.15), Basic (PF01586.12), CUT
706 (PF02376.11), DM (PF00751.14), Ets (PF00178.18), Forkhead (PF00250.14), GATA
707 (PF00320.23), GCM (PF03615.11), HLH (PF00010.22), HMG_box (PF00505.15),
708 Hairy_orange (PF07527.9), Homeobox (PF00046.25), Hormone_recep (PF00104.26),
709 OAR (PF03826.13), P53 (PF00870.14), P53_tetramer (PF07710.7), PAX (PF00292.14),

710 Pou (PF00157.13), HPD (PF05044.8), RHD_DNA_bind (PF00554.18), Runt
711 (PF00853.15), SCAN (PF02023.13), SIM_C (PF06621.8), SRF-TF (PF00319.14), T-box
712 (PF00907.18), TBX (PF12598.4), TF_AP-2 (PF03299.10), TF_Otx (PF03529.9), bZIP_1
713 (PF00170.17), bZIP_2 (PF07716.11), zf-C2H2 (PF00096.22), zf-C2HC (PF01530.14) and
714 zf-C4 (PF00105.14)

715

716 **4. OrthoFinder analysis**

717 OrthoFinder (version: 2.5.4, with default parameters) (Emms and Kelly 2019) was used to
718 examine the orthogroups (OGs) of NRs in the represented nematode species of five major
719 groups (Fig. 6): Rhabditina (*Ancylostoma ceylanicum*, *Caenorhabditis elegans*,
720 *Heligmosomoides polygyrus*, and *Pristionchus pacificus*), Tylenchina (*Globodera pallida*,
721 *Meloidogyne arenaria*, and *Steinernema monticolum*), Spirurina (*Ascaris suum* and *Brugia*
722 *malayi*), Trichinellida (*Trichuris muris*), and Enoplida (*Pontonema vulgare*). Peptide
723 sequences of NRs from each species were obtained as described above. After identifying
724 163 OGs in this comparison, we investigated the taxonomic origin of the genes in each OG
725 (Rhabditina, Tylenchina, Spirurina, Trichinellida, and Enoplida). If the OG contained one
726 or more genes from all taxa, the OG was considered to be the one that the common ancestor
727 of the taxa had (Fig. 6B). Using these criteria, the evolutionary gain/loss events of NR OGs
728 were resolved, as shown in Fig. 6B. Output file of the analysis is available in the
729 supplementary dataset.

730

731 **5. Transcriptome analysis**

732 *Data collection*

733 We collected transcriptome data, including molting stages, for a total of six nematode
734 species from public databases. The expression matrix (RPKM) for *Caenorhabditis elegans*
735 was obtained from Kim et al., 2013 (Gene Expression Omnibus, accession number:
736 GSE49043) (Kim, et al. 2013). WormBase ParaSite (version: WBPS19, WS291) (Howe,

et al. 2017) was also the resource of this study to obtain the calculated expression matrix (TPM) for *Trichuris suis* (NCBI Sequence Read Archive [SRA] accession number: SRP039506) and *Globodera pallida* (NCBI SRA accession number: ERP001236). The expression matrix (TPM) for *Pristionchus pacificus* was obtained from the supplementary file of Sun et al. 2021(Sun, et al. 2021). In addition, raw read data of *Brugia malayi* and *Ancylostoma ceylanicum* were obtained from SRA (NCBI SRA, accession number: SRR4308250-51 and SRR9858310-17 [*B. malayi*] (Grote, et al. 2020) and SRR2125572, SRR2125581-86, SRR2125588-90, SRR2125594, SRR2125597, SRR2125600, SRR2125602, SRR2125606-7, SRR2125610-SRR2125611, SRR2125614, and SRR2125627 [*A. ceylanicum*] (Bernot, et al. 2020)), and the expression levels were calculated by us. As mentioned above, quality control and filtering of raw reads were performed by FastQC and trimmomatic, respectively. We also used samtools (version: 1.15.1) to remove the ribosomal RNA-derived sequences in the *B. malayi (Danecek, et al. 2021)*. The filtered reads were mapped to the reference transcript models (*B. malayi*: PRJNA1072 and *A. ceylanicum*: PRJNA231479, WormBase Parasite (Howe, et al. 2017)) using RSEM/bowtie2 (version: v1.3.1, rsem-calculate-expression --paired-end --bowtie2) to calculate expression levels (TPM) (Li and Dewey 2011). Molting stages were referred from original/previous papers (Kim, et al. 2013; Cotton, et al. 2014; Leroux, et al. 2018; Bernot, et al. 2020; Grote, et al. 2020; Sun, et al. 2021; Shears and Grencis 2022). Expression levels of the transcripts corresponding to the *ecr* and *hr3,* which were identified in the above screenings, were obtained from each transcriptome dataset (the average of TPM was calculated in the case of having replicates at the same stage). In the transcriptome data of *G. pallida*, the gene model of *hr3* was inappropriately reconstructed into two models (id: GPLIN_000052400 and GPLIN_000052600). Thus, the expression levels were calculated by summing the expression levels of the two models at each time point. *grh-1* and *blmp-1* were annotated by reciprocal blast search (*B. malayi*: Gene:WBGene00226940 [*grh-1*], Gene:WBGene00223835 [*blmp-1*]; *A. ceylanicum*: Acey_s0568.v2.g2260 [*grh-1*], Acey_s0580.v2.g13356 [*blmp-1*]; *T. suis*: D918_02299 [*grh-1*], D918_01175 [*blmp-1*]; *P. pacificus*: PPA28052 [*grh-1*], PPA04978 [*blmp-1*]; *G. pallida*: GPLIN_000211500

766 [*grh-1*], GPLIN_000875200 [*blmp-1*]; and *C. elegans*: grh-1 [*grh-1*], blmp-1 [*blmp-1*]).
767 Their expression was investigated using the same dataset/methods (Fig. S11).

768

769 *Data curation*

770 Sun et al., 2021 originally provided the 1–2 h interval transcriptome data of *P. pacifucs*
771 from 0 to 58 h after hatching (i.e., 0, 1, 3, 5, ... 58 h) (Sun, et al. 2021). In our preliminary
772 analysis, we found that the data contained an overall fluctuating expression pattern
773 throughout the examined stages (Fig. S9A). Therefore, we divided the time points into
774 overlapping windows of three time points each, and the mean was calculated for each
775 window. For example, the first time-window was grouped by the data at 0, 1, and 3 h, and
776 the mean value represents the data at 1 h. The second window included the data at 1, 3, and
777 5 h, and the mean value represents the data at 3 h. Using this method, we obtained the
778 corrected expression profiles, which tends to remove the effects of fluctuating expression
779 due to biological or technical differences on individual development (Fig. S9B).

780

781 *Unbiased screening of NRs for identifying molting regulators*

782 With reference to our previous work (Yamakawa and Hejnol 2024), the expression profiles
783 (TPM matrices) of four nematode transcriptome data were classified into 5–7 clusters using
784 fuzzy c-mean clustering (Fig. S10: *A. ceylanicum*, *G. pallida*, *B. malayi*, and *T. suis*).
785 Analysis was carried out using R and its package e1071 (version: 1.7.11: https://cran.r-
786 project.org/web/packages/e1071/index.html). From such clustering, the genes in the
787 cluster(s) that showed a positively associated expression pattern with molting cycles were
788 extracted (Fig. S10, green shades, *A. ceylanicum*: 8110, *G. pallida*: 3383, *B. malayi*: 7114,
789 and *T. suis*: 2896 genes). In addition, Sun et al. 2021 and Kim et al. 2013 extracted the
790 genes whose expression showed an oscillatory pattern along the molting cycle in *P.*
791 *pacificus* (2,964 genes) and *C. elegans* (1,592 genes: assigned to clusters 1–6 in Kim et al.,
792 2013), respectively (Kim, et al. 2013; Sun, et al. 2021). As described above, OrthoFinder

793 (Emms and Kelly 2019) was used to extract OGs among the screened genes, and this result
794 identified 5,180 OGs. Among 5,180 OGs, 55 OGs contain one or more genes from all
795 species. We extracted 168 genes which were assigned into any 55 OGs in *C. elegans.*
796 Finally, we searched for the presence of TF and NR domains in the represented the *C.*
797 *elegans* 168 genes using Hmmer search (Johnson, et al. 2010) (see above).

798

799 **6. Prediction of heterodimer structure**

800 *Foldseek search for the identification of the candidate proteins*

801 First, we extracted the ligand-binding domain of USP from *Drosophila melanogaster*
802 (UniProt: P20153) using the NCBI Conserved Domain Search tool
803 (https://www.ncbi.nlm.nih.gov/Structure/cdd/wrpsb.cgi) (Blum, et al. 2024). We performed a
804 Foldseek Search on the Foldseek web server (https://search.foldseek.com/search) and
805 predicted the three-dimensional structure of USP with the 3Di/AA mode using sequence
806 information (van Kempen, et al. 2024). We used this prediction as a query and targeted the
807 AFDB-PROTEOME database in *C. elegans* (UP000001940). The results of this search are
808 shown in Table S3. Subsequent analysis focused on five candidate proteins (NHR-64,
809 NHR-69, NHR-35, NHR-49, and NHR-14). The orthologous genes were identified in
810 several nematode species using BLAST and phylogenetic analyses (Enoplida: *Pontonema*
811 *vulgare*, *Trissonchulus latispiculum*; Trichinellida: *Trichuris murris*; Dorylaimida:
812 *Mesodorylaimus YZB24*; Spirurina: *Ascaris suum* and *Brugia malayi*; Tylenchina:
813 *Globodera pallida*, *Steinernema monticolum*, and *Meloidogyne arenaria*; and Rhabditina:
814 *Caenorhabditis elegans*, *Heligmosomoides polygyrus*, *Ancylostoma ceylanicum*, and
815 *Pristionchus pacificus*). The phylogenetic tree is available in the supplementary dataset,
816 and Fig. S14 shows part of the tree (the USP and HNF4 clade).

817

818 *Prediction of heterodimer interaction*

819 The ColabFold interface was used to perform AlphaFold2 and AlphaFold2-Multimer
820 analyses (Evans, et al. 2022; Mirdita, et al. 2022). The sequences used in the analysis were
821 obtained from the above analysis or from UniProt (*D. melanogaster* ECR: P34021 and
822 HNF4: P49866). The ligand binding domains were extracted using the NCBI Conserved
823 Domain Search tool. The sequences were assigned to the ColabFold interface and analyzed
824 with the default settings (e.g., num_relax = 0 and template_mode = none). Five protein
825 structure models were predicted in each analysis. We presented the 3D model and ipTM
826 score of the most reliable model in the main text (Figs. 7 and S1). The 3D models of the
827 proteins were generated using PyMOL (version 3.1, https://www.pymol.org/), and the heat
828 maps were obtained from the ColabFold output files. The original output files of this
829 analysis are available in the supplementary dataset.

830

831 **7. TM-alignment**

832 *Extraction and prediction of NR and HNF4 LBDs*

833 The predicted protein structure datasets for *C. elegans* (UP000001940_6239_CAEEL_v6)
834 and *D. melanogaster* (UP000000803_7227_DROME_v6) were obtained from the
835 AlphaFold Protein Structure Database (Fleming, et al. 2025). The expanded HNF4 genes
836 of *C. elegans* were extracted by removing eight conserved non-HNF4 NR genes (*nhr-6*,
837 *nhr-8*, *nhr-23*, *nhr-25*, *nhr-41*, *nhr-67*, *nhr-85*, and *nhr-91*) from the NR genes annotated
838 as nuclear hormone receptors (*nhr-1*, *nhr-2*, …). The NRs of *D. melanogaster* were
839 extracted based on previous annotations in UniProt (P16376: 7UP2, Q9VML1: DSF,
840 P13055: E75, P45447: E78, and P34021: ECR, Q8WS79: ERR, Q05192: FTF1B, and
841 P33244: FTZF1, P49866: HNF4, P31396: HR3, P49869: HR38, Q9W539: HR4, A1ZA01:
842 HR51, Q24142: HR78, Q9VI12: HR83, Q24143: HR96, P18102: TLL, and P20153: USP).
843 We used the NCBI Conserved Domain Search
844 (https://www.ncbi.nlm.nih.gov/Structure/cdd/wrpsb.cgi) with the default settings to
845 identify the NR LBD (ligand binding domain) in each protein sequence. Note that we
846 removed genes with LBD regions of 150 amino acids or fewer to focus on genes with

847 functional LBDs and reduce artificial errors. Finally, we extracted the structures of the
848 specific LBD regions from each dataset using pdb-tools (218 and 16 proteins in *C. elegans*
849 and *D. melanogaster*, respectively) (Rodrigues, et al. 2018).

850 Unlike *C. elegans* and *D. melanogaster*, the predicted protein structure of
851 *Meloidogyne incognita* was not available in a public database, so we predicted the protein
852 structure of *M. incognita* HNF4s. As mentioned above, 175 NRs were extracted from the
853 *M. incognita* genome, and a phylogenetic analysis was performed on all NRs and reference
854 NR proteins (500 bootstrap replications, the reconstructed tree is available in the
855 supplementary dataset). We removed 24 non-HNF4 NRs, and the LBD regions were
856 investigated in the remaining 151 proteins. Subsequently, LBD sequences were obtained
857 for 64 proteins with more than 150 amino acid residues in the LBD. We predicted each
858 protein structure using ColabFold/Alphafold2, as mentioned above. We applied the same
859 analysis to HNF4 proteins from other nematodes. For example, we extracted HNF4
860 proteins from 28 species of Chromadorida, Desmodorida, Dioctophymatida, Dorylaimida,
861 Enoplida, Mermithida, Monhysterida, and Trichinellida. Gene identity was confirmed by
862 BLAST-based search (ex., reciprocal tophit with *D. melanogaster* HNF4). Finally, the
863 HNF4 LBD structure was predicted in 20 species (*Epsilonema ZAB2, Pontonema vulgare,*
864 *Ptycholaimellus GST110, Rhynchonema JSB14, Soboliphyme baturini, Trichinella T6, T.*
865 *T8, T. T9, T. britovi, T. murrelli, T. nativa, T. nelsoni, T. papuae, T. patagoniensis, T.*
866 *pseudospiralis, T. zimbabwensis, Trissonchulus WLG14,* and *Trissonchulus latispiculum*).
867 In subsequent analyses, we used the best-predicted models for each prediction.
868

869 *Scoring of TM-align*

870 Using the above three protein structure datasets (nematode "ancestral" HNF4, *C. elegans*
871 expanded HNF4, and *M. incognita* expanded HNF4 proteins), we performed pairwise TM-
872 align (version: 20220412) analysis with reference *D. melanogaster* NR proteins (Zhang
873 and Skolnick 2005). The analysis was performed without any additional options. We used
874 the normalized TM-score with nematode HNF4 proteins to generate a TM-score heatmap

875 and histograms. The results, including the script and raw TM-scores, are available in the
876 supplementary dataset.

877

878 **8. Yeast two-hybrid assay**

879 A yeast two-hybrid assay was performed using the Matchmaker Gold Yeast Two-Hybrid
880 System (Takara Bio, Shiga, Japan). In brief, the target sequences were inserted into the bait
881 and prey vector plasmids (pGBKT7 and pGADT7, respectively). The plasmids were then
882 co-transformed into the Y2HGold yeast strain and cultured on selective agar plates.

883

884 *Amplification of the target sequences and plasmid construction*

885 We commercially purchased *D. melanogaster* from Easy Zoo GmbH (Minden, Germany),
886 and 5–15 pupae and adults were homogenized with liquid nitrogen and TRIzol Reagent
887 (Invitrogen, MA, USA) to extract total RNA. The total RNA was collected using 1-bromo-
888 3-chloropropane and further purified using isopropanol precipitation methods. After
889 DNase treatment (Thermo Scientific, MA, USA), the RNA solution underwent further
890 purification with ethanol precipitation. We applied the same methods to *C. elegans* worms
891 of mixed stages. Reverse transcription and cDNA synthesis were conducted using a
892 RevertAid First Strand cDNA Synthesis Kit (Thermo Scientific, MA, USA) by following
893 the provided protocol. LBDs of *D. melanogaster ecr*, *usp*, *hnf4*, *C. elegans nhr-64*, and
894 *nhr-69* were predicted as mentioned above. The primers used to amplify the LBD regions
895 with additional sequence for plasmid construction are shown in Table S5. The pGBKT7
896 and pGADT7 plasmids were linearized by inverse PCR using the specific primers designed
897 in the multiple cloning sites (see Table S5). The amplified and purified DNA fragments
898 were cloned into the linearized plasmids using an In-Fusion Cloning Kit (Takara Bio).
899 Accuracy of the insertion was confirmed by colony PCR and direct sequencing.

900

901 *Co-transformation and detection of the protein interactions*

902 The above plasmids were co-transformed into the yeast Y2HGold using the Yeastmaker
903 Yeast Transformation System 2 (Takara Bio). The procedure was followed by the provided
904 protocol. Liquid YPDA medium was used to grow the yeast cultures, and the
905 transformation was performed with a standard lithium acetate method. See the main text
906 for the bait/prey pairs of co-transformations. We used pGBKT7-53, pGBKT7-Lam, and
907 pGADT7-T vectors, which were provided in the same kit, for positive/negative control. As
908 shown in Fig. S15G, Y2HGold is auxotrophic for adenine (Ade), histidine (His), leucine
909 (Leu), and tryptophan (Trp), and pGBKT7 and pGADT7 vector complements Trp and Leu,
910 respectively. Thus, the co-transformants were first obtained by streaking the treated yeasts
911 into the SD-Leu-Trp, and well-grown colonies were subsequently streaked onto the
912 selective agar plates to test the expression of other reporter genes. In our preliminary
913 screening, the test using the reporter gene *ADE2* is too strict to detect the interaction of our
914 target proteins. For example, although the colonies of the co-transformants of p53-T were
915 found on SD-Leu-Trp-His-Ade, no colonies of the co-transformants of DmECR-DmUSP,
916 whose interaction was previously reported, were found. Thus, we decided to target the
917 HIS3 and MEL1 reporter genes, whose stringency is comparatively mild, by using SD-
918 Leu-Trp-His/X-alpha-gal plates (Fig. S15G). Specifically, the co-transformants were
919 spread on SD-Leu-Trp for three days, and each of 6–12 well-grown colonies were further
920 stroked onto SD-Leu-Trp/X-alpha-gal. We tested whether the colonies further amplify and
921 turn to blue color within 24–48h. We used the following materials for making the agar
922 plates: Minimal SD Base (Takara Bio), DO Supplement -Leu/-Trp (Takara Bio), DO
923 Supplement -Ade/-His/-Leu/-Trp (Takara Bio), 5-Bromo-4-chloro-3-indolyl α-D-
924 galactopyranoside (=X-alpha-gal, Sigma-Aldrich), and Adenine Hemisulfate Salt (Sigma-
925 Aldrich).

926

927 **9. Culture of nematodes and pharmacological experiments**

928 *Culture of C. elegans*, *D. pachys*, and *P. sambesii*

929 We used *C. elegans* (N2 lineage), which were kept at the Institute of Nutritional Science
930 in Friedrich Schiller University Jena, Germany. *D. pachys* and *P. sambesii* were obtained
931 from Prof. Dr. Ralf Schnabel (Institute of Genetics, TU Braunschweig, Germany). They
932 are cultured at room temperature on the optimized agar plates for each species. For *C.*
933 *elegans,* we used a standard NGM/nematode growth media plate (Stiernagle 2006). *D.*
934 *pachys* were cultured on the 2% agar plate in tap water, which was obtained in our lab
935 (Institute of Zoology and Evolutionary Research, Friedrich Schiller University Jena,
936 Germany). The agar solution was poured onto the plates without adding any materials after
937 autoclaving. The plate for *P. sambesii* was made of 2% agar in distilled water. 5 g/L
938 cholesterol (Carl ROTH, Karlsruhe, Germany) was made in 96% ethanol, and the 1/1000
939 amount of cholesterol solution was added to the agar solution after autoclaving. All of the
940 three species are bacterial feeders, and we provided the *E. coli* OP50 to *C. elegans* and *P.*
941 *sambesii*, and *E. coli* HT115 to *D. pachys*. The above cultivation methods for *D. pachys*
942 and *P. sambesii* was kindly advised by Prof. Dr. Ralf Schnabel. Except the above
943 differences in agar plates and bacterial food, manipulation and maintenance were followed
944 by the manual of *C. elegans* (Stiernagle 2006).

945

946 *Collection of synchronous L1 worms*

947 With reference to the methods in *C. elegans* (Stiernagle 2006), synchronous L1 worms of
948 each species were obtained by bleaching gravid adults or eggs, which were laid on the agar
949 plates. A bleaching solution was made of a 2:1:2 mix solution of a hygiene cleaner, which
950 was commercially purchased (DanKlorix, Colgate-Palmolive Deutschland GmbH,
951 Germany), 10N NaOH solution, and M9 buffer, respectively. The worms and eggs were
952 collected by washing the plate surface with 2–5 ml M9 buffer (several hundred-thousand
953 worms in total). We also used a drawing brush to effectively collect the eggs which were
954 laid beneath the agar surface in *D. pachys* and *P. sambesii*. The M9 buffers with worms
955 and eggs were washed with M9 buffer two times using a centrifuge (12,000 g; for 30–60
956 sec), and finally, the solution was concentrated to around 100–500 µl. Two-times volume

957 of the freshly made bleaching solution was added to the concentrated M9 buffer. The
958 bleaching process was carried out in the 1.5 ml tube or small Petri dishes. In any case, the
959 solutions were periodically shaken with pipetting or vortexing, and the bleaching process
960 was carefully monitored using microscopes until most of the worm bodies were dissolved.
961 Although the duration of bleaching was dependent on the species and the number of the
962 worms, it usually took 5–15 min until we ceased the bleaching process. Before removing
963 the bleaching solution by centrifuge, since eggs of some species (especially *P. sambesii*)
964 did not sink to the bleaching solution, we added the same amount of M9 buffer.
965 Subsequently, the eggs were washed with M9 buffer and centrifuged (12,000 g; for 30–60
966 sec) two-three times and further concentrated to 100–200 µl. Finally, the obtained solutions
967 with eggs were placed onto the plain agar plates, which are optimized to each species. The
968 solution was not sprayed to the plate, but spotted at a central part; the plate was also slowly
969 dried in the clean bench. Within two to three days, the L1 worms hatched and moved from
970 the area where the buffer solution was originally placed. We collected the L1 worms by
971 removing the spotted area and washing with M9 buffer solution. We found that many *D.*
972 *pachys* and *P. sambesii* worms did not survive in the M9 buffer without streaking onto
973 plain agar plates.

974

975 *Observation of molting process and staging*

976 We began culturing of collected synchronous L1 worms by transferring them to an agar
977 plate with an OP50 or HT115 lawn. To observe molting stages and perform
978 pharmacological analysis, the worms were cultured at 20°C. We anesthetized the worms
979 using sodium azide and observed the worms on the agar plate for differential interference
980 constrast (DIC) imaging. We characterized the larval stages of *D. pachys* and *P. sambesii*
981 based on observations of gonadal development, with reference to the previous reports on
982 the same genus species (Tahseen, et al. 1991; TAHsEEN, et al. 1992; Hubbard and
983 Greenstein 2000; Schindler and Sherwood 2013). As shown in Fig. S7A–C, gonadal
984 primordia can be observed even in L1 worms. The primordia enlarge in the L2 stage and

985 elongate further in the L3 stage. During the L4 stage, the primordiaelongate significantly,
986 and the developed vulva can also be clearly observed. Adult worms can easily be
987 distinguished by observing the developed gonads containing eggs. Male worms are very
988 rare in all examined species, and we focused on hermaphroditic adults of *C. elegans* and
989 parthenogenetic adults of *D. pachys* and *P. sambesii*. Nevertheless, since it is difficult to
990 distinguish the sex of the worms during early larval stages (e.g., L1 and L2), L1 worms
991 were used for the subsequent analysis without classifying their sex. We confirmed that the
992 worms developed "female" morphology.

993

994 *Pharmacological analysis*

995 We commercially purchased cucurbitacin B (CucB, CAS number: 6199-67-3) from
996 TargetMol (Wellesley Hills, MA, USA). We prepared a 50 mM stock solution of CucB in
997 DMSO, and the experiments were performed in four-well plates. We added 500 µl of warm
998 agar solution into a well after autoclaving, and 5 µl of CucB or DMSO was also added and
999 mixed well before the agar hardened. In our preliminary tests, 50 µM is the highest
1000 concentration which can be solved in the agar plate. Subsequently, the bacterial food (10
1001 µl in LB liquid culture) was added on the surface of the agar. Note that we used the
1002 optimized agar plates for culturing each species. Finally, synchronous L1 worms were
1003 transferred to the agar plates, and the plates were placed in the dark for two or three days
1004 at 20°C. For the experiments targeting the L3–L4 molting of *P. sambesii*, we used worms
1005 cultured for four days, as shown above. The periods of drug treatment are shown in Figs
1006 3C and S7A. The morphology of the treated worms was observed as mentioned above. The
1007 larval and adult stages of the worms were also determined using the previously mentioned
1008 criteria. We judged the separation of old cuticles from the body as the apolysis process. We
1009 counted the number of worms that developed into landmark stages (shown in Fig. 3C) and
1010 the number of worms in the process of apolysis. All processes were repeated three times
1011 (three replicates), and the raw results are shown in Table S2. We performed a statistical
1012 analysis (Student's t-test) using R (version 4.3.3).

10. Data visualization

We used R (version: 4.3.3) (Team 2024) and its packages such as Tydyverse (version: 2.0.0) (Wickham, et al. 2019), ggtree (version: 3.10.1) (Xu, et al. 2022), ggstance (version: 0.3.7, https://github.com/lionel-/ggstance), ggvenn (version: 0.1.10, https://github.com/yanlinlin82/ggvenn), and ape (version: 5.8, https://cran.r-project.org/web/packages/ape/index.html) to analyze and visualize the results. Images for Fig. S6 are from PHYLOPIC (https://www.phylopic.org/).

11. Data availability

Scripts and datasets (e.g. assembly sequences, phylogenetic trees, data accession numbers) are available in the supplementary dataset.

Acknowledgments

We thank all current and former member of the Hejnol laboratory. In particular, we thank Nina Levin for proofreading of the manuscript. This study was supported by JSPS Oversea Fellowship (Japan Society for the Promotion of Science, to S.Y.), IMPULSE project (Friedrich Schiller University Jena, to S.Y.), Deutsche Forschungsgemeinschaft (project number 519107654, to A.H.), and the HFSP grant (RGP0041/2022, to A.H.).

Supplementary information

Supplementary dataset

Supplementary figures (S1–S15, see the attached PDF file)

Supplementary tables (S1–S5, see the attached excel file)

1038 **References**

1039 Adams S, Pathak P, Shao H, Lok JB, Pires-daSilva A. 2019. Liposome-based transfection enhances RNAi
1040 and CRISPR-mediated mutagenesis in non-model nematode systems. *Sci Rep.* **9**:483. 10.1038/s41598-018-
1041 37036-1

1042 Aguinaldo AMA, Turbeville JM, Linford LS, Rivera MC, Garey JR, Raff RA, Lake JA. 1997. Evidence for
1043 a clade of nematodes, arthropods and other moulting animals. *Nature.* **387**:489-493.

1044 Ahmed M, Roberts NG, Adediran F, Smythe AB, Kocot KM, Holovachov O. 2022. Phylogenomic Analysis
1045 of the Phylum Nematoda: Conflicts and Congruences With Morphology, 18S rRNA, and Mitogenomes.
1046 *Frontiers in Ecology and Evolution.* **9**. 10.3389/fevo.2021.769565

1047 Álvarez-Ortega S, Brito JA, Subbotin SA. 2019. Multigene phylogeny of root-knot nematodes and molecular
1048 characterization of Meloidogyne nataliei Golden, Rose & Bird, 1981 (Nematoda: Tylenchida). *Scientific*
1049 *Reports.* **9**:11788. 10.1038/s41598-019-48195-0

1050 Antebi A. 2015. Nuclear receptor signal transduction in C. elegans. *WormBook.* **1**.

1051 Banerjee D, Kwok A, Lin S-Y, Slack FJ. 2005. Developmental Timing in C. elegans Is Regulated by kin-20
1052 and tim-1, Homologs of Core Circadian Clock Genes. *Developmental Cell.* **8**:287-295.
1053 https://doi.org/10.1016/j.devcel.2004.12.006

1054 Barker GC, Mercer JG, Rees HH, Howells RE. 1991. The effect of ecdysteroids on the microfilarial
1055 production ofBrugia pahangi and the control of meiotic reinitiation in the oocytes ofDirofilaria immitis.
1056 *Parasitology Research.* **77**:65-71. 10.1007/BF00934388

1057 Bernot JP, Rudy G, Erickson PT, Ratnappan R, Haile M, Rosa BA, Mitreva M, O'Halloran DM, Hawdon
1058 JM. 2020. Transcriptomic analysis of hookworm Ancylostoma ceylanicum life cycle stages reveals changes
1059 in G-protein coupled receptor diversity associated with the onset of parasitism. *International Journal for*
1060 *Parasitology.* **50**:603-610. https://doi.org/10.1016/j.ijpara.2020.05.003

1061 Bitra K, Palli SR. 2009. Interaction of proteins involved in ecdysone and juvenile hormone signal
1062 transduction. *Arch Insect Biochem Physiol.* **70**:90-105. 10.1002/arch.20281

1063 Blum M, Andreeva A, Florentino Laise C, Chuguransky Sara R, Grego T, Hobbs E, Pinto Beatriz L, Orr A,
1064 Paysan-Lafosse T, Ponamareva I, et al. 2024. InterPro: the protein sequence classification resource in 2025.
1065 *Nucleic Acids Research.* **53**:D444-D456. 10.1093/nar/gkae1082

1066 Bolger AM, Lohse M, Usadel B. 2014. Trimmomatic: a flexible trimmer for Illumina sequence data.
1067 *Bioinformatics.* **30**:2114-2120.

1068 Bonneton F, Chaumot A, Laudet V. 2008. Annotation of Tribolium nuclear receptors reveals an increase in
1069 evolutionary rate of a network controlling the ecdysone cascade. *Insect Biochem Mol Biol.* **38**:416-429.
1070 10.1016/j.ibmb.2007.10.006

1071 Browning C, McEwen AG, Mori K, Yokoi T, Moras D, Nakagawa Y, Billas IML. 2021. Nonsteroidal
1072 ecdysone receptor agonists use a water channel for binding to the ecdysone receptor complex EcR/USP. *J*
1073 *Pestic Sci.* **46**:88-100. 10.1584/jpestics.D20-095

1074 Cao M. 2023. CRISPR-Cas9 genome editing in Steinernema entomopathogenic nematodes.
1075 *bioRxiv.*2023.2011.2024.568619. 10.1101/2023.11.24.568619

1076 Capella-Gutiérrez S, Silla-Martínez JM, Gabaldón T. 2009. trimAl: a tool for automated alignment trimming
1077 in large-scale phylogenetic analyses. *Bioinformatics.* **25**:1972-1973. 10.1093/bioinformatics/btp348

1078 Chitwood DJ, Feldlaufer MF. 1990. Ecdysteroids in Axenically Propagated Caenorhabditis elegans and
1079 Culture Medium. *J Nematol.* **22**:598-607.

1080 Cleator M, Delves CJ, Howells RE, Rees HH. 1987. Identity and tissue localization of free and conjugated
1081 ecdysteroids in adults of Dirofilaria immitis and Ascaris suum. *Molecular and Biochemical Parasitology.*
1082 **25**:93-105. https://doi.org/10.1016/0166-6851(87)90022-3

1083 Cotton JA, Lilley CJ, Jones LM, Kikuchi T, Reid AJ, Thorpe P, Tsai IJ, Beasley H, Blok V, Cock PJA, et al.
1084 2014. The genome and life-stage specific transcriptomes of Globodera pallidaelucidate key aspects of plant
1085 parasitism by a cyst nematode. *Genome Biology.* **15**:R43. 10.1186/gb-2014-15-3-r43

1086 Cunha TJ, de Medeiros BAS, Lord A, Sørensen MV, Giribet G. 2023. Rampant loss of universal metazoan
1087 genes revealed by a chromosome-level genome assembly of the parasitic Nematomorpha. *Current Biology.*
1088 **33**:3514-3521.e3514. https://doi.org/10.1016/j.cub.2023.07.003

1089 Danecek P, Bonfield JK, Liddle J, Marshall J, Ohan V, Pollard MO, Whitwham A, Keane T, McCarthy SA,
1090 Davies RM, et al. 2021. Twelve years of SAMtools and BCFtools. *Gigascience.* **10**.
1091 10.1093/gigascience/giab008

1092 Dayi M, Kanzaki N, Sun S, Ide T, Tanaka R, Masuya H, Okabe K, Kajimura H, Kikuchi T. 2021. Additional
1093 description and genome analyses of Caenorhabditis auriculariae representing the basal lineage of genus
1094 Caenorhabditis. *Scientific Reports.* **11**:6720. 10.1038/s41598-021-85967-z

1095 Delves CJ, Howells RE, Post RJ. 1986. Gametogenesis and fertilization in Dirofilaria immitis (Nematoda:
1096 Filarioidea). *Parasitology.* **92**:181-197. 10.1017/S003118200006354X

1097 Dennis RD. 1976. Insect morphogenetic hormones and developmental mechanisms in the nematode,
1098 Nematospiroides dubius. *Comparative Biochemistry and Physiology Part A: Physiology.* **53**:53-56.
1099 https://doi.org/10.1016/S0300-9629(76)80009-6

1100 Dumidae A, Luangsawang K, Thanwisai A, Vitta A. 2023. Identification and genetic characterization of
1101 Angiostrongylus cantonensis isolated from the human eye. *Parasitology Research.* **122**:2217-2225.
1102 10.1007/s00436-023-07922-3

1103 Dunn CW, Hejnol A, Matus DQ, Pang K, Browne WE, Smith SA, Seaver E, Rouse GW, Obst M, Edgecombe
1104 GD. 2008. Broad phylogenomic sampling improves resolution of the animal tree of life. *Nature.* **452**:745-
1105 749.

1106 Eleftheriadi K, Guiglielmoni N, Salces-Ortiz J, Vargas-Chavez C, Martínez-Redondo GI, Gut M, Flot J-F,
1107 Schmidt-Rhaesa A, Fernández R. (10_24072_pcjournal_381 co-authors). 2024. The genome sequence of the
1108 Montseny horsehair worm, Gordionus montsenyensis sp. nov., a key resource to investigate Ecdysozoa
1109 evolution. *Peer Community Journal.* **4**. 10.24072/pcjournal.381

1110 Emms DM, Kelly S. 2019. OrthoFinder: phylogenetic orthology inference for comparative genomics.
1111 *Genome Biology.* **20**:1-14.

1112 Evans R, O'Neill M, Pritzel A, Antropova N, Senior A, Green T, Žídek A, Bates R, Blackwell S, Yim J, et
1113 al. 2022. Protein complex prediction with AlphaFold-Multimer. *bioRxiv.*2021.2010.2004.463034.
1114 10.1101/2021.10.04.463034

1115 Evershed RP, Mercer JG, Rees HH. 1987. Capillary gas chromatography-mass spectrometry of ecdysteroids.
1116 *Journal of Chromatography A.* **390**:357-369. https://doi.org/10.1016/S0021-9673(01)94387-0

1117 Fleming J, Magana P, Nair S, Tsenkov M, Bertoni D, Pidruchna I, Lima Afonso MQ, Midlik A, Paramval
1118 U, Žídek A, et al. 2025. AlphaFold Protein Structure Database and 3D-Beacons: New Data and Capabilities.
1119 *Journal of Molecular Biology.* **437**:168967. https://doi.org/10.1016/j.jmb.2025.168967

1120 Fleming MW. 1985. Ascaris suum: role of ecdysteroids in molting. *Exp Parasitol.* **60**:207-210.
1121 10.1016/0014-4894(85)90024-4

1122 Fleming MW. 1993. Ecdysteroids during development in the ovine parasitic nematode, Haemonchus
1123 contortus. *Comparative Biochemistry and Physiology Part B: Comparative Biochemistry.* **104**:653-655.
1124 https://doi.org/10.1016/0305-0491(93)90192-8

1125 Frand AR, Russel S, Ruvkun G. 2005. Functional Genomic Analysis of C. elegans Molting. *PLOS Biology.*
1126 **3**:e312. 10.1371/journal.pbio.0030312

1127 Gao Y, Zhang X, Wei J, Sun X, Yuan J, Li F, Xiang J. 2015. Whole Transcriptome Analysis Provides Insights
1128 into Molecular Mechanisms for Molting in Litopenaeus vannamei. *PLoS One.* **10**:e0144350.
1129 10.1371/journal.pone.0144350

1130 Giribet G, Edgecombe GD. 2017. Current Understanding of Ecdysozoa and its Internal Phylogenetic
1131 Relationships. *Integrative and Comparative Biology.* **57**:455-466. 10.1093/icb/icx072

1132 Gissendanner CR, Crossgrove K, Kraus KA, Maina CV, Sluder AE. 2004. Expression and function of
1133 conserved nuclear receptor genes in Caenorhabditis elegans. *Developmental Biology.* **266**:399-416.
1134 https://doi.org/10.1016/j.ydbio.2003.10.014

1135 Gonzalez Akimori D, Dalessandro EJ, Nolan TJ, Stieha CR, Lok JB, Stoltzfus JDC. 2021. Transcriptional
1136 profiles in Strongyloides stercoralis males reveal deviations from the Caenorhabditis sex determination
1137 model. *Scientific Reports.* **11**:8254. 10.1038/s41598-021-87478-3

1138 Graham LD, Kotze AC, Fernley RT, Hill RJ. 2010. An ortholog of the ecdysone receptor protein (EcR) from
1139 the parasitic nematode Haemonchus contortus. *Molecular and Biochemical Parasitology.* **171**:104-107.
1140 https://doi.org/10.1016/j.molbiopara.2010.03.003

1141 Grote A, Li Y, Liu C, Voronin D, Geber A, Lustigman S, Unnasch TR, Welch L, Ghedin E. 2020. Prediction
1142 pipeline for discovery of regulatory motifs associated with Brugia malayi molting. *PLOS Neglected Tropical*
1143 *Diseases.* **14**:e0008275. 10.1371/journal.pntd.0008275

1144 Hada K, Asahina M, Hasegawa H, Kanaho Y, Slack FJ, Niwa R. 2010. The nuclear receptor gene nhr-25
1145 plays multiple roles in the Caenorhabditis elegans heterochronic gene network to control the larva-to-adult
1146 transition. *Developmental Biology.* **344**:1100-1109.

1147 Hauser YP, Meeuse MWM, Gaidatzis D, Großhans H. 2022. The BLMP-1 transcription factor promotes
1148 oscillatory gene expression to achieve timely molting. *bioRxiv.*2021.2007.2005.450828.
1149 10.1101/2021.07.05.450828

1150 Hayes GD, Frand AR, Ruvkun G. 2006. The mir-84 and let-7 paralogous microRNA genes of Caenorhabditis
1151 elegans direct the cessation of molting via the conserved nuclear hormone receptors NHR-23 and NHR-25.
1152 *Development.* **133**:4631-4641. 10.1242/dev.02655

1153 Hejnol A, Obst M, Stamatakis A, Ott M, Rouse GW, Edgecombe GD, Martinez P, Baguñà J, Bailly X,
1154 Jondelius U. 2009. Assessing the root of bilaterian animals with scalable phylogenomic methods.
1155 *Proceedings of the Royal Society B: Biological Sciences.* **276**:4261-4270.

1156 Hellekes V, Claus D, Seiler J, Illner F, Schiffer PH, Kroiher M. 2023. CRISPR/Cas9 mediated gene editing
1157 in non-model nematode Panagrolaimus sp. PS1159. *Front Genome Ed.* **5**:1078359.
1158 10.3389/fgeed.2023.1078359

1159 Hendriks GJ, Gaidatzis D, Aeschimann F, Großhans H. 2014. Extensive oscillatory gene expression during
1160 C. elegans larval development. *Mol Cell.* **53**:380-392. 10.1016/j.molcel.2013.12.013

1161 Henschel R, Lieber M, Wu L-S, Nista PM, Haas BJ, LeDuc RD editors. Proceedings of the 1st Conference
1162 of the Extreme Science and Engineering Discovery Environment: Bridging from the eXtreme to the campus
1163 and beyond. 2012.

1164 Herranz M, Stiller J, Worsaae K, Sørensen MV. 2022. Phylogenomic analyses of mud dragons
1165 (Kinorhyncha). *Molecular Phylogenetics and Evolution.* **168**:107375.
1166 https://doi.org/10.1016/j.ympev.2021.107375

1167 Hill RJ, Billas IM, Bonneton F, Graham LD, Lawrence MC. 2013. Ecdysone receptors: from the Ashburner
1168 model to structural biology. *Annu Rev Entomol.* **58**:251-271. 10.1146/annurev-ento-120811-153610

1169 Hiroki S, Yoshitane H. 2024. Ror homolog nhr-23 is essential for both developmental clock and circadian
1170 clock in C. elegans. *Communications Biology.* **7**:243. 10.1038/s42003-024-05894-3

1171 Howe KL, Bolt BJ, Shafie M, Kersey P, Berriman M. 2017. WormBase ParaSite − a comprehensive resource
1172 for helminth genomics. *Molecular and Biochemical Parasitology.* **215**:2-10.
1173 https://doi.org/10.1016/j.molbiopara.2016.11.005

1174 Hu L, Zhang M, Sun Y, Bu Y. 2020. Characterization and phylogenetic analysis of the first complete
1175 mitochondrial genome of Cylicocyclus radiatus. *Veterinary Parasitology.* **281**:109097.
1176 https://doi.org/10.1016/j.vetpar.2020.109097

1177 Hubbard EJA, Greenstein D. 2000. The Caenorhabditis elegans gonad: a test tube for cell and developmental
1178 biology. *Developmental dynamics: an official publication of the American Association of Anatomists.* **218**:2-
1179 22.

1180 Hyde CJ, Elizur A, Ventura T. 2019. The crustacean ecdysone cassette: A gatekeeper for molt and
1181 metamorphosis. *The Journal of Steroid Biochemistry and Molecular Biology.* **185**:172-183.

1182 Johnson LC, Vo AA, Clancy JC, Myles KM, Pooranachithra M, Aguilera J, Levenson MT, Wohlenberg C,
1183 Rechtsteiner A, Ragle JM, et al. 2023. NHR-23 activity is necessary for C. elegans developmental
1184 progression and apical extracellular matrix structure and function. *Development.* **150**. 10.1242/dev.201085

1185 Johnson LS, Eddy SR, Portugaly E. 2010. Hidden Markov model speed heuristic and iterative HMM search
1186 procedure. *BMC bioinformatics.* **11**:1-8.

1187 Jumper J, Evans R, Pritzel A, Green T, Figurnov M, Ronneberger O, Tunyasuvunakool K, Bates R, Žídek A,
1188 Potapenko A, et al. 2021. Highly accurate protein structure prediction with AlphaFold. *Nature.* **596**:583-589.
1189 10.1038/s41586-021-03819-2

1190 Katoh K, Standley DM. 2013. MAFFT multiple sequence alignment software version 7: improvements in
1191 performance and usability. *Mol Biol Evol.* **30**:772-780. 10.1093/molbev/mst010

1192 Kim D, Grün D, van Oudenaarden A. 2013. Dampening of expression oscillations by synchronous regulation
1193 of a microRNA and its target. *Nat Genet.* **45**:1337-1344. 10.1038/ng.2763

1194 Kinney B, Sahu S, Stec N, Hills-Muckey K, Adams DW, Wang J, Jaremko M, Joshua-Tor L, Keil W,
1195 Hammell CM. 2023. A circadian-like gene network programs the timing and dosage of heterochronic miRNA
1196 transcription during C. elegans development. *Dev Cell.* **58**:2563-2579.e2568. 10.1016/j.devcel.2023.08.006

1197 Kostrouchova M, Kostrouch Z. 2015. Nuclear receptors in nematode development: Natural experiments
1198 made by a phylum. *Biochimica et Biophysica Acta (BBA) - Gene Regulatory Mechanisms.* **1849**:224-237.
1199 https://doi.org/10.1016/j.bbagrm.2014.06.016

1200 Kostrouchova M, Krause M, Kostrouch Z, Rall JE. 1998. CHR3: a Caenorhabditis elegans orphan nuclear
1201 hormone receptor required for proper epidermal development and molting. *Development.* **125**:1617-1626.
1202 10.1242/dev.125.9.1617

1203 Kostrouchova M, Krause M, Kostrouch Z, Rall JE. 2001. Nuclear hormone receptor CHR3 is a critical
1204 regulator of all four larval molts of the nematode Caenorhabditis elegans. *Proc Natl Acad Sci U S A.* **98**:7360-
1205 7365. 10.1073/pnas.131171898

1206 Kouns NA, Nakielna J, Behensky F, Krause MW, Kostrouch Z, Kostrouchova M. 2011. NHR-23 dependent
1207 collagen and hedgehog-related genes required for molting. *Biochem Biophys Res Commun.* **413**:515-520.
1208 10.1016/j.bbrc.2011.08.124

1209 Kozlova T, Thummel CS. 2000. Steroid Regulation of Postembryonic Development and Reproduction in
1210 Drosophila. *Trends in Endocrinology & Metabolism.* **11**:276-280. https://doi.org/10.1016/S1043-
1211 2760(00)00282-4

1212 Lachaise F, Le Roux A, Hubert M, Lafont R. 1993. The molting gland of crustaceans: localization, activity,
1213 and endocrine control (a review). *Journal of Crustacean Biology.* **13**:198-234.

1214 Lai C-K, Lee Y-C, Ke H-M, Lu MR, Liu W-A, Lee H-H, Liu Y-C, Yoshiga T, Kikuchi T, Chen PJ, et al.
1215 2022. The Aphelenchoides genomes reveal substantial horizontal gene transfers in the last

common ancestor of free-living and major plant parasitic nematodes. *bioRxiv.*2022.2009.2013.507733. 10.1101/2022.09.13.507733

Lamberti ML, Spangler RK, Cerdeira V, Ares M, Rivollet L, Ashley GE, Coronado AR, Tripathi S, Spiousas I, Ward JD, et al. 2024. Clock gene homologs lin-42 and kin-20 regulate circadian rhythms in C. elegans. *Scientific Reports.* **14**:12936. 10.1038/s41598-024-62303-9

Leroux LP, Nasr M, Valanparambil R, Tam M, Rosa BA, Siciliani E, Hill DE, Zarlenga DS, Jaramillo M, Weinstock JV, et al. 2018. Analysis of the Trichuris suis excretory/secretory proteins as a function of life cycle stage and their immunomodulatory properties. *Sci Rep.* **8**:15921. 10.1038/s41598-018-34174-4

Lezzi M, Bergman T, Henrich VC, Vögtli M, Frömel C, Grebe M, Przibilla S, Spindler-Barth M. 2002. Ligand-induced heterodimerization between the ligand binding domains of the Drosophila ecdysteroid receptor and ultraspiracle. *Eur J Biochem.* **269**:3237-3245. 10.1046/j.1432-1033.2002.03001.x

Li B, Dewey CN. 2011. RSEM: accurate transcript quantification from RNA-Seq data with or without a reference genome. *BMC bioinformatics.* **12**:1-16.

Liang B, Ferguson K, Kadyk L, Watts JL. 2010. The role of nuclear receptor NHR-64 in fat storage regulation in Caenorhabditis elegans. *PLoS One.* **5**:e9869. 10.1371/journal.pone.0009869

Lindblom TH, Dodd AK. 2006. Xenobiotic detoxification in the nematode Caenorhabditis elegans. *J Exp Zool A Comp Exp Biol.* **305**:720-730. 10.1002/jez.a.324

Lindblom TH, Pierce GJ, Sluder AE. 2001. A C. elegans orphan nuclear receptor contributes to xenobiotic resistance. *Curr Biol.* **11**:864-868. 10.1016/s0960-9822(01)00236-6

Liu L, Liu X, Fu Y, Fang W, Wang C. 2022. Whole-body transcriptome analysis provides insights into the cascade of sequential expression events involved in growth, immunity, and metabolism during the molting cycle in Scylla paramamosain. *Scientific Reports.* **12**:11395. 10.1038/s41598-022-14783-w

Malakhov U. 1986. Nematodes: Structure, development, classification and phylogeny.

McCann K, Grant W, Doyle S. 2021. The genome sequence of the Australian filarial nematode, Cercopithifilaria johnstoni [version 2; peer review: 3 approved]. *Wellcome Open Research.* **6**. 10.12688/wellcomeopenres.17258.2

Meeuse MW, Hauser YP, Morales Moya LJ, Hendriks GJ, Eglinger J, Bogaarts G, Tsiairis C, Großhans H. 2020. Developmental function and state transitions of a gene expression oscillator in Caenorhabditis elegans. *Mol Syst Biol.* **16**:e9498. 10.15252/msb.20209498

Meeuse MWM, Hauser YP, Nahar S, Smith AAT, Braun K, Azzi C, Rempfler M, Großhans H. 2023. C. elegans molting requires rhythmic accumulation of the Grainyhead/LSF transcription factor GRH-1. *Embo j.* **42**:e111895. 10.15252/embj.2022111895

Mhashilkar AS, Vankayala SL, Liu C, Kearns F, Mehrotra P, Tzertzinis G, Palli SR, Woodcock HL, Unnasch TR. 2016. Identification of Ecdysone Hormone Receptor Agonists as a Therapeutic Approach for Treating Filarial Infections. *PLOS Neglected Tropical Diseases.* **10**:e0004772. 10.1371/journal.pntd.0004772

Mirdita M, Schütze K, Moriwaki Y, Heo L, Ovchinnikov S, Steinegger M. 2022. ColabFold: making protein folding accessible to all. *Nature Methods.* **19**:679-682. 10.1038/s41592-022-01488-1

Monsalve GC, Van Buskirk C, Frand AR. 2011. LIN-42/PERIOD controls cyclical and developmental progression of C. elegans molts. *Curr Biol.* **21**:2033-2045. 10.1016/j.cub.2011.10.054

Murai Y, Yagi-Utsumi M, Fujiwara M, Tanaka S, Tomita M, Kato K, Arakawa K. 2021. Multiomics study of a heterotardigrade, Echinisicus testudo, suggests the possibility of convergent evolution of abundant heat-soluble proteins in Tardigrada. *BMC Genomics.* **22**:813. 10.1186/s12864-021-08131-x

Nielsen C. 2012. Animal evolution: interrelationships of the living phyla: Oxford University Press.

Niwa R, Niwa YS. 2014. Enzymes for ecdysteroid biosynthesis: their biological functions in insects and beyond. *Bioscience, biotechnology, and biochemistry.* **78**:1283-1292.

1261 Öztürk-Çolak A, Marygold SJ, Antonazzo G, Attrill H, Goutte-Gattat D, Jenkins VK, Matthews BB,
1262 Millburn G, dos Santos G, Tabone CJ, et al. 2024. FlyBase: updates to the Drosophila genes and genomes
1263 database. *Genetics.* **227**. 10.1093/genetics/iyad211

1264 Parihar M, Minton RL, Flowers S, Holloway A, Morehead BE, Paille J, Gissendanner CR. 2010. The genome
1265 of the nematode Pristionchus pacificus encodes putative homologs of RXR/Usp and EcR. *General and*
1266 *Comparative Endocrinology.* **167**:11-17. https://doi.org/10.1016/j.ygcen.2010.02.005

1267 Patel R, Galagali H, Kim JK, Frand AR. 2022. Feedback between a retinoid-related nuclear receptor and the
1268 let-7 microRNAs controls the pace and number of molting cycles in C. elegans. *Elife.* **11**.
1269 10.7554/eLife.80010

1270 Pathare PP, Lin A, Bornfeldt KE, Taubert S, Van Gilst MR. 2012. Coordinate Regulation of Lipid
1271 Metabolism by Novel Nuclear Receptor Partnerships. *PLOS Genetics.* **8**:e1002645.
1272 10.1371/journal.pgen.1002645

1273 Patil G, van Zon JS. 2024. Timers, variability, and body-wide coordination: C. elegans as a model system for
1274 whole-animal developmental timing. *Curr Opin Genet Dev.* **85**:102172. 10.1016/j.gde.2024.102172

1275 Patke A, Young MW, Axelrod S. 2020. Molecular mechanisms and physiological importance of circadian
1276 rhythms. *Nature reviews Molecular cell biology.* **21**:67-84.

1277 Qing X, Zhang YM, Sun S, Ahmed M, Lo W-S, Bert W, Holovachov O, Li H. 2024. Phylogenomic Insights
1278 into the Evolution and Origin of Nematoda. *Systematic Biology.* **74**:349-358. 10.1093/sysbio/syae073

1279 Rhodehouse K, Cascino K, Aseltine L, Padula A, Weinstein R, Spina JS, Olivero CE, Van Wynsberghe PM.
1280 2018. The Doubletime Homolog KIN-20 Mainly Regulates let-7 Independently of Its Effects on the Period
1281 Homolog LIN-42 in Caenorhabditis elegans. *G3 (Bethesda).* **8**:2617-2629. 10.1534/g3.118.200392

1282 Rodrigues J, Teixeira J, Trellet M, Bonvin A. 2018. pdb-tools: a swiss army knife for molecular structures
1283 [version 1; peer review: 2 approved]. *F1000Research.* **7**. 10.12688/f1000research.17456.1

1284 Schindler AJ, Sherwood DR. 2013. Morphogenesis of the caenorhabditis elegans vulva. *Wiley Interdiscip*
1285 *Rev Dev Biol.* **2**:75-95. 10.1002/wdev.87

1286 Schumann I, Kenny N, Hui J, Hering L, Mayer G. 2018. Halloween genes in panarthropods and the evolution
1287 of the early moulting pathway in Ecdysozoa. *R Soc Open Sci.* **5**:180888. 10.1098/rsos.180888

1288 Schwarz EM, Baniya A, Heppert JK, Schwartz HT, Tan C-H, Antoshechkin I, Sternberg PW, Goodrich-Blair
1289 H, Dillman AR. 2025. Genomes of the entomopathogenic nematode Steinernema
1290 hermaphroditum and its associated bacteria. *bioRxiv.*2025.2001.2009.632278.
1291 10.1101/2025.01.09.632278

1292 Shea C, Hough D, Xiao J, Tzertzinis G, Maina CV. 2004. An rxr/usp homolog from the parasitic nematode,
1293 Dirofilaria immitis. *Gene.* **324**:171-182.

1294 Shea C, Richer J, Tzertzinis G, Maina CV. 2010. An EcR homolog from the filarial parasite, Dirofilaria
1295 immitis requires a ligand-activated partner for transactivation. *Molecular and Biochemical Parasitology.*
1296 **171**:55-63.

1297 Shears RK, Grencis RK. 2022. Whipworm secretions and their roles in host-parasite interactions. *Parasites*
1298 *& Vectors.* **15**:348. 10.1186/s13071-022-05483-5

1299 Smythe AB, Holovachov O, Kocot KM. 2019. Improved phylogenomic sampling of free-living nematodes
1300 enhances resolution of higher-level nematode phylogeny. *BMC Evolutionary Biology.* **19**:121.
1301 10.1186/s12862-019-1444-x

1302 Soriano IR, Riley IT, Potter MJ, Bowers WS. 2004. Phytoecdysteroids: A Novel Defense Against Plant-
1303 Parasitic Nematodes. *Journal of Chemical Ecology.* **30**:1885-1899. 10.1023/B:JOEC.0000045584.56515.11

Spangler RK, Braun K, Ashley GE, van der Does M, Wruck D, Coronado AR, Matthew Ragle J, Iesmantavicius V, Morales Moya LJ, Jonnalagadda K, et al. 2024. A conserved chronobiological complex times C. elegans development. *bioRxiv.* 10.1101/2024.05.09.593322

Stamatakis A. 2014. RAxML version 8: a tool for phylogenetic analysis and post-analysis of large phylogenies. *Bioinformatics.* **30**:1312-1313.

Stiernagle T. 2006. Maintenance of C. elegans. *WormBook.*1-11. 10.1895/wormbook.1.101.1

Subramoniam T. 2000. Crustacean ecdysteriods in reproduction and embryogenesis. *Comparative Biochemistry and Physiology Part C: Pharmacology, Toxicology and Endocrinology.* **125**:135-156. https://doi.org/10.1016/S0742-8413(99)00098-5

Sun S, Rödelsperger C, Sommer RJ. 2021. Single worm transcriptomics identifies a developmental core network of oscillating genes with deep conservation across nematodes. *Genome Res.* **31**:1590-1601. 10.1101/gr.275303.121

Sural S, Hobert O. 2021. Nematode nuclear receptors as integrators of sensory information. *Current Biology.* **31**:4361-4366.e4362. 10.1016/j.cub.2021.07.019

TAHsEEN Q, Ahmad I, Shamim Jairajpuri M. 1992. Description and developmental biology of Plectus zelli n. sp.(Nematoda: Araeolaimida). *Fundamental & Applied Nematology.* **15**:503-510.

Tahseen Q, Shamim Jairajpuri M, Ahmad I. 1991. Observations on the embryonic and post-embryonic development of Diploscapter orientalis (Nematoda: Rhabditida). *Revue de Nématologie.* **14**:251-260.

Taubenheim J, Kortmann C, Fraune S. 2021. Function and Evolution of Nuclear Receptors in Environmental-Dependent Postembryonic Development. *Frontiers in Cell and Developmental Biology.* **9**. 10.3389/fcell.2021.653792

Taubert S, Ward JD, Yamamoto KR. 2011. Nuclear hormone receptors in nematodes: evolution and function. *Mol Cell Endocrinol.* **334**:49-55. 10.1016/j.mce.2010.04.021

Team RC. 2024. R: A language and environment for statistical computing. R Foundation for Statistical Computing, Vienna, Austria.

Thummel CS. 1996. Flies on steroids — Drosophila metamorphosis and the mechanisms of steroid hormone action. *Trends in Genetics.* **12**:306-310. https://doi.org/10.1016/0168-9525(96)10032-9

Toyofuku M, Fujinaga D, Inaba K, Funahashi T, Fujikawa Y, Inoue H, Kataoka H, Niwa R, Ono H. 2021. The plant-derived triterpenoid, cucurbitacin B, but not cucurbitacin E, inhibits the developmental transition associated with ecdysone biosynthesis in Drosophila melanogaster. *Journal of Insect Physiology.* **134**:104294. https://doi.org/10.1016/j.jinsphys.2021.104294

Tsiairis C, Großhans H. 2021. Gene expression oscillations in C. elegans underlie a new developmental clock. *Curr Top Dev Biol.* **144**:19-43. 10.1016/bs.ctdb.2020.11.001

Tzertzinis G, Egaña AL, Palli SR, Robinson-Rechavi M, Gissendanner CR, Liu C, Unnasch TR, Maina CV. 2010. Molecular Evidence for a Functional Ecdysone Signaling System in Brugia malayi. *PLOS Neglected Tropical Diseases.* **4**:e625. 10.1371/journal.pntd.0000625

van Kempen M, Kim SS, Tumescheit C, Mirdita M, Lee J, Gilchrist CLM, Söding J, Steinegger M. 2024. Fast and accurate protein structure search with Foldseek. *Nature Biotechnology.* **42**:243-246. 10.1038/s41587-023-01773-0

Vogeler S, Galloway TS, Lyons BP, Bean TP. 2014. The nuclear receptor gene family in the Pacific oyster, Crassostrea gigas, contains a novel subfamily group. *BMC Genomics.* **15**:369. 10.1186/1471-2164-15-369

Warbrick EV, Barker GC, Rees HH, Howells RE. 1993. The effect of invertebrate hormones and potential hormone inhibitors on the third larval moult of the filarial nematode, Dirofilaria immitis, in vitro. *Parasitology.* **107**:459-463. 10.1017/S0031182000067822

Wickham H, Averick M, Bryan J, Chang W, McGowan LDA, François R, Grolemund G, Hayes A, Henry L, Hester J. 2019. Welcome to the Tidyverse. *Journal of open source software.* **4**:1686.

Xu S, Li L, Luo X, Chen M, Tang W, Zhan L, Dai Z, Lam TT, Guan Y, Yu G. 2022. Ggtree: A serialized data object for visualization of a phylogenetic tree and annotation data. *iMeta.* **1**:e56. https://doi.org/10.1002/imt2.56

Yamakawa S, Hejnol A. 2024. Ecdysteroid-dependent molting in tardigrades. *Current Biology.* **34**:p5804-5812.e5804. 10.1016/j.cub.2024.10.054

Yamakawa S, Yamazaki A, Morino Y, Wada H. 2023. Early expression onset of tissue-specific effector genes during the specification process in sea urchin embryos. *EvoDevo.* **14**:7. 10.1186/s13227-023-00210-2

Yamanaka N, Rewitz KF, O'Connor MB. 2013. Ecdysone control of developmental transitions: lessons from Drosophila research. *Annual review of entomology.* **58**:497-516.

Zhang Y, Skolnick J. 2005. TM-align: a protein structure alignment algorithm based on the TM-score. *Nucleic Acids Res.* **33**:2302-2309. 10.1093/nar/gki524

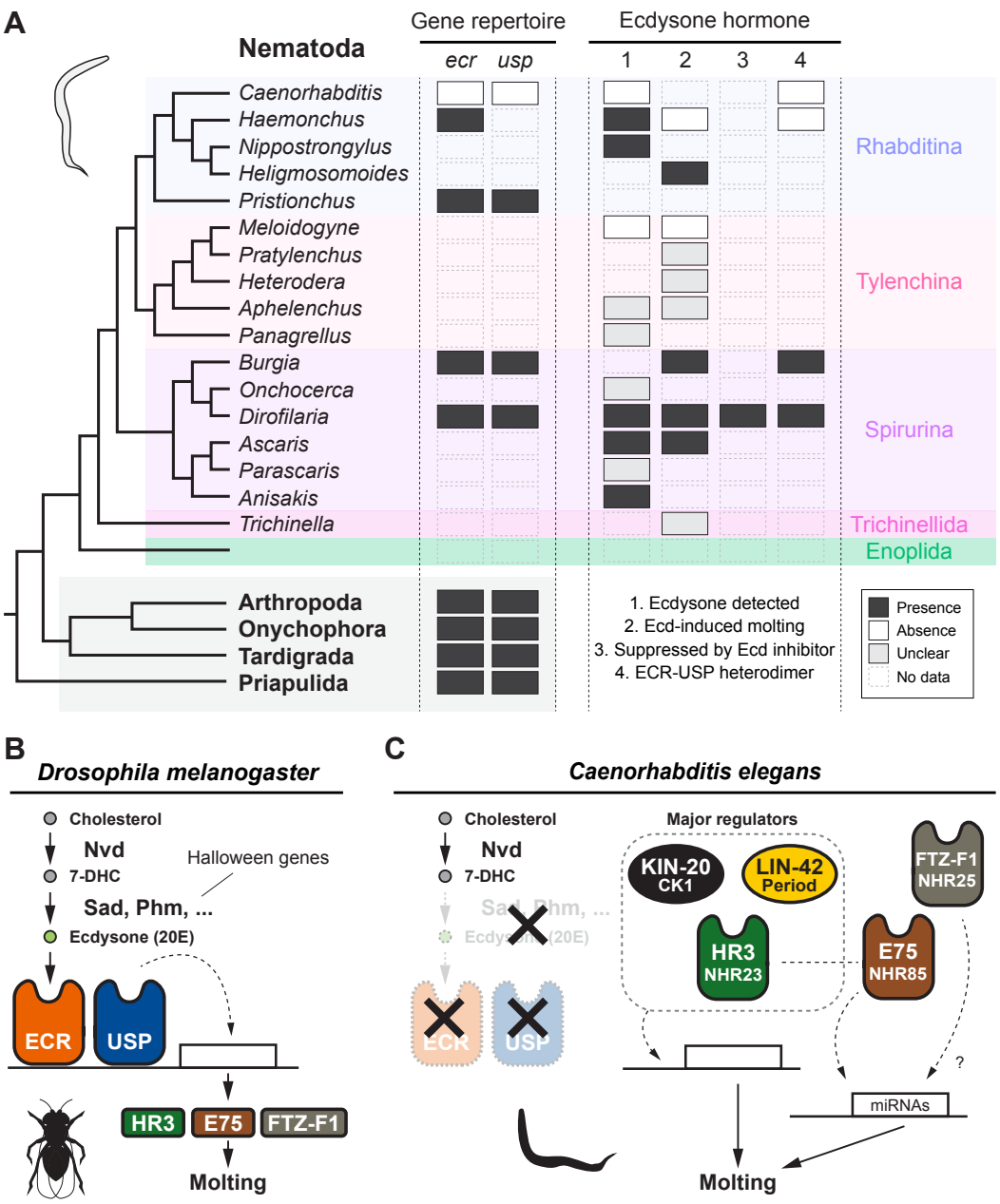
A
Nematoda
Gene repertoire
ecr
usp
Ecdysone hormone
1
2
3
4
Caenorhabditis
Haemonchus
Nippostrongylus
Heligmosomoides
Pristionchus
Meloidogyne
Pratylenchus
Heterodera
Aphelenchus
Panagrellus
Burgia
Onchocerca
Dirofilaria
Ascaris
Parascaris
Anisakis
Trichinella
Rhabditina
Tylenchina
Spirurina
Trichinellida
Enoplida
Arthropoda
Onychophora
Tardigrada
Priapulida
1. Ecdysone detected
2. Ecd-induced molting
3. Suppressed by Ecd inhibitor
4. ECR-USP heterodimer
Presence
Absence
Unclear
No data
B
Drosophila melanogaster
Cholesterol
Nvd
7-DHC
Halloween genes
Sad, Phm, ...
Ecdysone (20E)
ECR
USP
HR3
E75
FTZ-F1
Molting
C
Caenorhabditis elegans
Cholesterol
Nvd
7-DHC
Sad, Phm, ...
Ecdysone (20E)
ECR
USP
Major regulators
KIN-20
CK1
LIN-42
Period
FTZ-F1
NHR25
HR3
NHR23
E75
NHR85
?
miRNAs
Molting

1369 **Figure 1. An overview of previous work on the role of ecdysone hormone and molting**
1370 **regulation in nematodes and arthropods**
1371 **A**: (left two columns) Presence and absence of the ecdysone receptor (*ecr*) and its
1372 heterodimer partner gene *usp* in ecdysozoan taxa. (right four column) A summary of the
1373 findings on ecdysone hormonal control in nematodes. 1: detection of ecdysteroid hormone
1374 in the internal body, 2: molting induction by exogenous ecdysteroids (=Ecd), 3: molting
1375 suppression by exogenous ecdysteroid antagonists, and 4: the functionality of ECR-USP
1376 heterodimer. As shown in the legends of the panels, black, white, gray, and empty boxes
1377 indicate the presence, absence, unclear, and no information, respectively. **B** and **C**:
1378 Schematic diagrams of the molting regulatory mechanisms in *Drosophila melanogaster*
1379 and *Caenorhabditis elegans*, respectively. 20E (20-hydroxyecdysone) is synthesized from
1380 cholesterol by the Nvd and Halloween genes, such as Sad (Shadow) and Phm (Phantom).
1381 The ECR-USP heterodimer binds to 20E, activating a cascade of downstream genes,
1382 including HR3, E75, and FTZ-F1. *C. elegans* is known to lack genes that synthesize
1383 ecdysone and its receptors, which play an important regulatory role in insect molting. See
1384 the main text for details on each regulatory mechanism. The reference and the details of **A**
1385 are shown in Table S1.

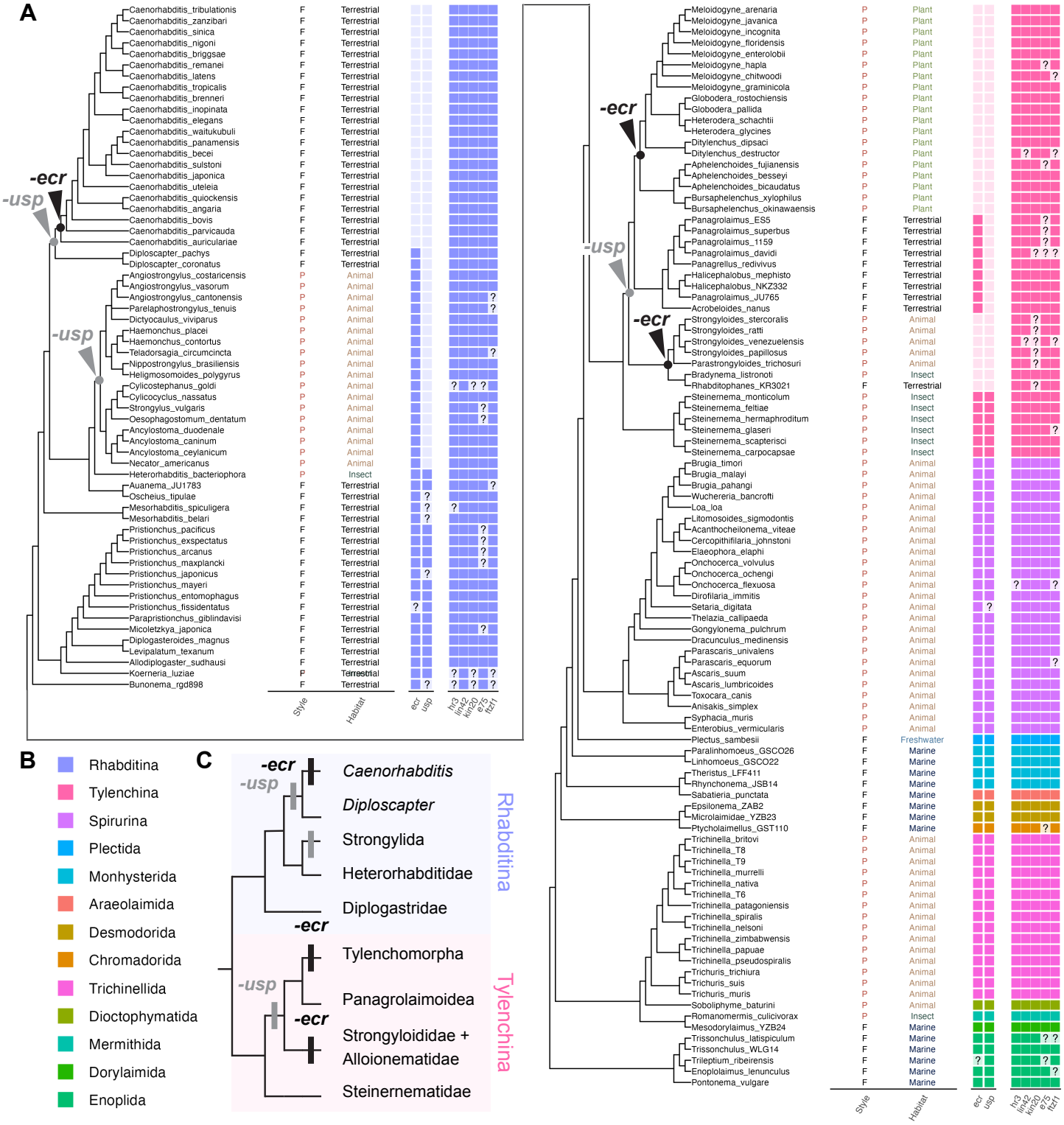
A
-ecr
-usp
-usp
-ecr
-usp
-ecr
Caenorhabditis_tribulationis
Caenorhabditis_zanzibari
Caenorhabditis_sinica
Caenorhabditis_nigoni
Caenorhabditis_briggsae
Caenorhabditis_remanei
Caenorhabditis_latens
Caenorhabditis_tropicalis
Caenorhabditis_brenneri
Caenorhabditis_inopinata
Caenorhabditis_elegans
Caenorhabditis_waitukubuli
Caenorhabditis_panamensis
Caenorhabditis_becei
Caenorhabditis_sulstoni
Caenorhabditis_japonica
Caenorhabditis_uteleia
Caenorhabditis_quiockensis
Caenorhabditis_angaria
Caenorhabditis_bovis
Caenorhabditis_parvicauda
Caenorhabditis_auriculariae
Diploscapter_pachys
Diploscapter_coronatus
Angiostrongylus_costaricensis
Angiostrongylus_vasorum
Angiostrongylus_cantonensis
Parelaphostrongylus_tenuis
Dictyocaulus_viviparus
Haemonchus_placei
Haemonchus_contortus
Teladorsagia_circumcincta
Nippostrongylus_brasiliensis
Heligmosomoides_polygyrus
Cylicostephanus_goldi
Cylicocyclus_nassatus
Strongylus_vulgaris
Oesophagostomum_dentatum
Ancylostoma_duodenale
Ancylostoma_caninum
Ancylostoma_ceylanicum
Necator_americanus
Heterorhabditis_bacteriophora
Auanema_JU1783
Oscheius_tipulae
Mesorhabditis_spiculigera
Mesorhabditis_belari
Pristionchus_pacificus
Pristionchus_exspectatus
Pristionchus_arcanus
Pristionchus_maxplancki
Pristionchus_japonicus
Pristionchus_mayeri
Pristionchus_entomophagus
Pristionchus_fissidentatus
Parapristionchus_giblindavisi
Micoletzkya_japonica
Diplogasteroides_magnus
Levipalatum_texanum
Allodiplogaster_sudhausi
Koerneria_luziae
Bunonema_rgd898
Meloidogyne_arenaria
Meloidogyne_javanica
Meloidogyne_incognita
Meloidogyne_floridensis
Meloidogyne_enterolobii
Meloidogyne_hapla
Meloidogyne_chitwoodi
Meloidogyne_graminicola
Globodera_rostochiensis
Globodera_pallida
Heterodera_schachtii
Heterodera_glycines
Ditylenchus_dipsaci
Ditylenchus_destructor
Aphelenchoides_fujianensis
Aphelenchoides_besseyi
Aphelenchoides_bicaudatus
Bursaphelenchus_xylophilus
Bursaphelenchus_okinawaensis
Panagrolaimus_ES5
Panagrolaimus_superbus
Panagrolaimus_1159
Panagrolaimus_davidi
Panagrellus_redivivus
Halicephalobus_mephisto
Halicephalobus_NKZ332
Panagrolaimus_JU765
Acrobeloides_nanus
Strongyloides_stercoralis
Strongyloides_ratti
Strongyloides_venezuelensis
Strongyloides_papillosus
Parastrongyloides_trichosuri
Bradynema_listronoti
Rhabditophanes_KR3021
Steinernema_monticolum
Steinernema_feltiae
Steinernema_hermaphroditum
Steinernema_glaseri
Steinernema_scapterisci
Steinernema_carpocapsae
Brugia_timori
Brugia_malayi
Brugia_pahangi
Wuchereria_bancrofti
Loa_loa
Litomosoides_sigmodontis
Acanthocheilonema_viteae
Cercopithifilaria_johnstoni
Elaeophora_elaphi
Onchocerca_volvulus
Onchocerca_ochengi
Onchocerca_flexuosa
Dirofilaria_immitis
Setaria_digitata
Thelazia_callipaeda
Gongylonema_pulchrum
Dracunculus_medinensis
Parascaris_univalens
Parascaris_equorum
Ascaris_suum
Ascaris_lumbricoides
Toxocara_canis
Anisakis_simplex
Syphacia_muris
Enterobius_vermicularis
Plectus_sambesii
Paralinhomoeus_GSCO26
Linhomoeus_GSCO22
Theristus_LFF411
Rhynchonema_JSB14
Sabatieria_punctata
Epsilonema_ZAB2
Microlaimidae_YZB23
Ptycholaimellus_GST110
Trichinella_britovi
Trichinella_T8
Trichinella_T9
Trichinella_murrelli
Trichinella_nativa
Trichinella_T6
Trichinella_patagoniensis
Trichinella_spiralis
Trichinella_nelsoni
Trichinella_zimbabwensis
Trichinella_papuae
Trichinella_pseudospiralis
Trichuris_trichiura
Trichuris_suis
Trichuris_muris
Soboliphyme_baturini
Romanomermis_culicivorax
Mesodorylaimus_YZB24
Trissonchulus_latispiculum
Trissonchulus_WLG14
Trileptium_ribeirensis
Enoplolaimus_lenunculus
Pontonema_vulgare
Style
Habitat
ecr
usp
hr3
lin42
kin20
e75
ftz1
B
Rhabditina
Tylenchina
Spirurina
Plectida
Monhysterida
Araeolaimida
Desmodorida
Chromadorida
Trichinellida
Dioctophymatida
Mermithida
Dorylaimida
Enoplida
C
-ecr
-usp
Caenorhabditis
Diploscapter
Strongylida
Heterorhabditidae
Diplogastridae
-ecr
Tylenchomorpha
-usp
Panagrolaimoidea
-ecr
Strongyloididae +
Alloionematidae
Steinernematidae
Rhabditina
Tylenchina

1386 **Figure 2. Gene repertory of the target genes (*ecr, usp, hr3, kin-20 lin-42, e75, and ftz-*
1387 ***f1)* in 160 nematode species**
1388 **A**: Lifestyle (P: parasite and F: free-living), habitat, and gene repertories (*ecr, usp, hr3, lin-*
1389 *42, kin-20, e75, and ftz-f1*) are indicated with the phylogeny of the target nematode species
1390 (color represents the taxa, question marks represent missing information). The nodes of *ecr*
1391 and *usp* loss events are highlighted in the tree. **B**: Legends for color and taxa. **C**: A simpler
1392 tree clarifying the loss of ECR and USP in the Rhabditina and Tylenchina groups
1393
1394

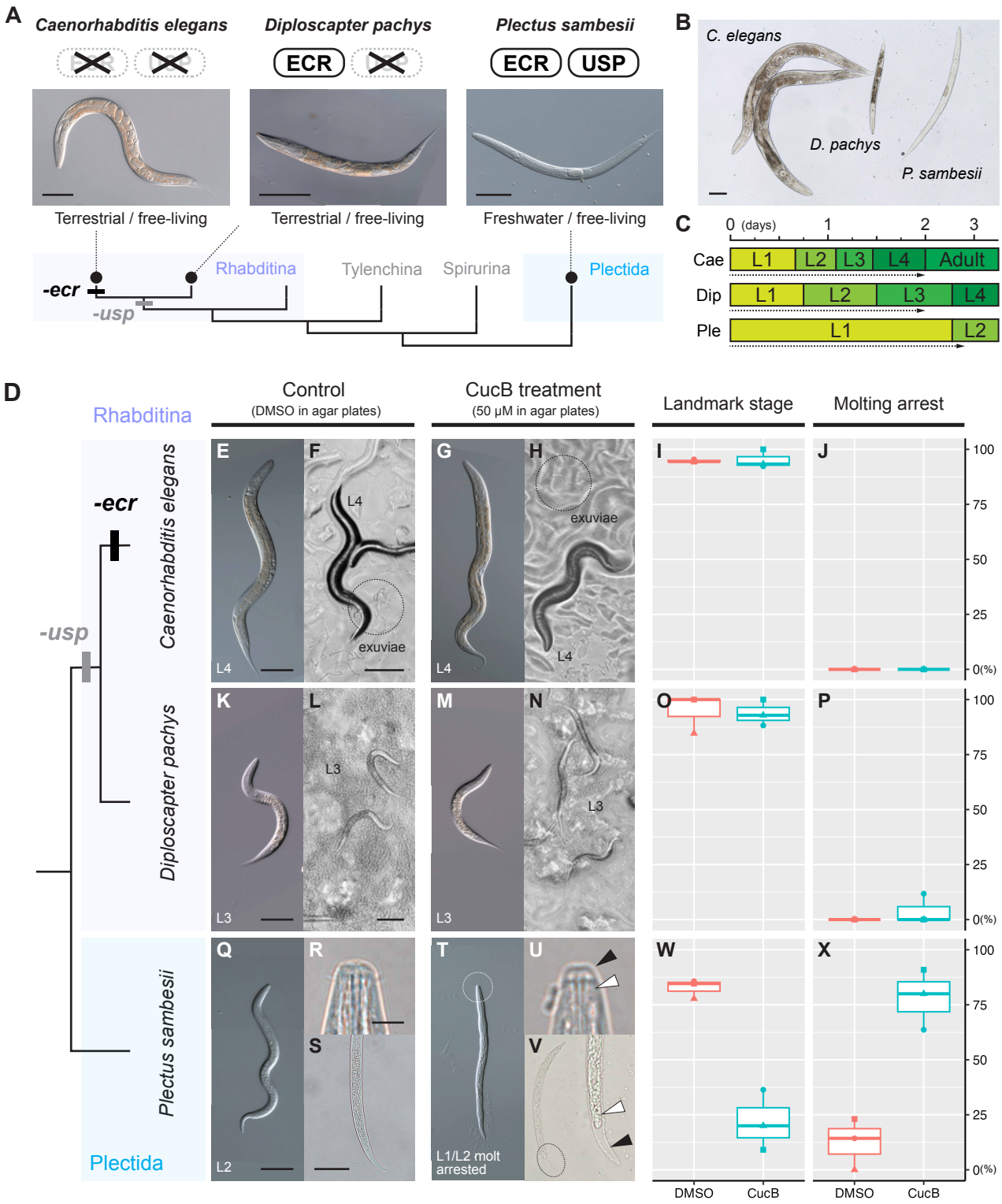
A
Caenorhabditis elegans
Diploscapter pachys
Plectus sambesii
ECR
ECR
USP
Terrestrial / free-living
Terrestrial / free-living
Freshwater / free-living
-ecr
-usp
Rhabditina
Tylenchina
Spirurina
Plectida
B
C. elegans
D. pachys
P. sambesii
C
0 (days)
1
2
3
Cae
L1
L2
L3
L4
Adult
Dip
L1
L2
L3
L4
Ple
L1
L2
D
Rhabditina
Control
(DMSO in agar plates)
CucB treatment
(50 µM in agar plates)
Landmark stage
Molting arrest
-ecr
-usp
Caenorhabditis elegans
Diploscapter pachys
Plectus sambesii
Plectida
E
F
G
H
I
J
L4
exuviae
K
L
M
N
O
P
L3
Q
R
S
T
U
V
W
X
L2
L1/L2 molt arrested
100
75
50
25
0(%)
DMSO
CucB

1395 **Figure 3. Effects of the ECR antagonist, Cucurbitacin B, treatment on the molting**
1396 **process in *Caenorhabditis elegans*, *Diploscapter pachys,* and *Plectus sambesii***

1397 **A**: The phylogeny of the *ecr*/*usp* repertoire in the three target species. The photos show the
1398 adult gravid worms with eggs (scale bars: 100 µm). **B**: A comparison of body size among
1399 representative adult individuals of the three species (scale bar: 100 µm). **C**: Growth speed
1400 and molting timing after feeding on L1 worms in each species (Cae: *C. elegans*; Dip: *D.*
1401 *pachys*; and Ple: *P. sambesii*). L1–L4 represent the first to fourth larval stages. See the
1402 Methods and Fig. S7 for detailed information about larval and adult staging. Dotted arrows
1403 indicate the duration of cucurbitacin B (CucB) treatment. **D**–**X:** the results of CucB
1404 treatment. **D** shows the phylogeny of the target species. The results for *C. elegans*, *D.*
1405 *pachys*, and *P. sambesii* are shown in **E**–**J**, **K**–**P**, and **Q**–**X**, respectively. Representative
1406 worms after DMSO treatment are shown in **E**–**F**, **K**–**L**, and **Q**–**S**; CucB: **G**–**H**, **M**–**N**, and
1407 **T**–**V**. **E**, **G**, **K**, **M**, **Q**, and **T**: DIC images of the treated worms; **F**, **H**, **L**, and **N**; the worms
1408 on agar plates; **R**, **S**, **U**, and **V**: magnified images of the mouth (**R** and **U**) and tail (**S** and
1409 **V**) parts, indicating the process of apolysis during CucB treatment (the black and white
1410 arrowheads indicate the old and new cuticles, respectively). Scale bars for **E**/**G**, **F**/**H**, and
1411 **L**/**N**: 100 µm; for **K**/**M**, **Q**/**T**, and **S**/**V**: 50 µm; and for **R**/**U**: 5 µm. **I**, **Q**, and **W**: the
1412 percentage of DMSO- or CucB-treated worms that developed to the landmark stage. **J**, **P**,
1413 and **X:** the percentage of DMSO- or CucB-treated worms that showed molting arrest/defect
1414 phenotypes.
1415
1416

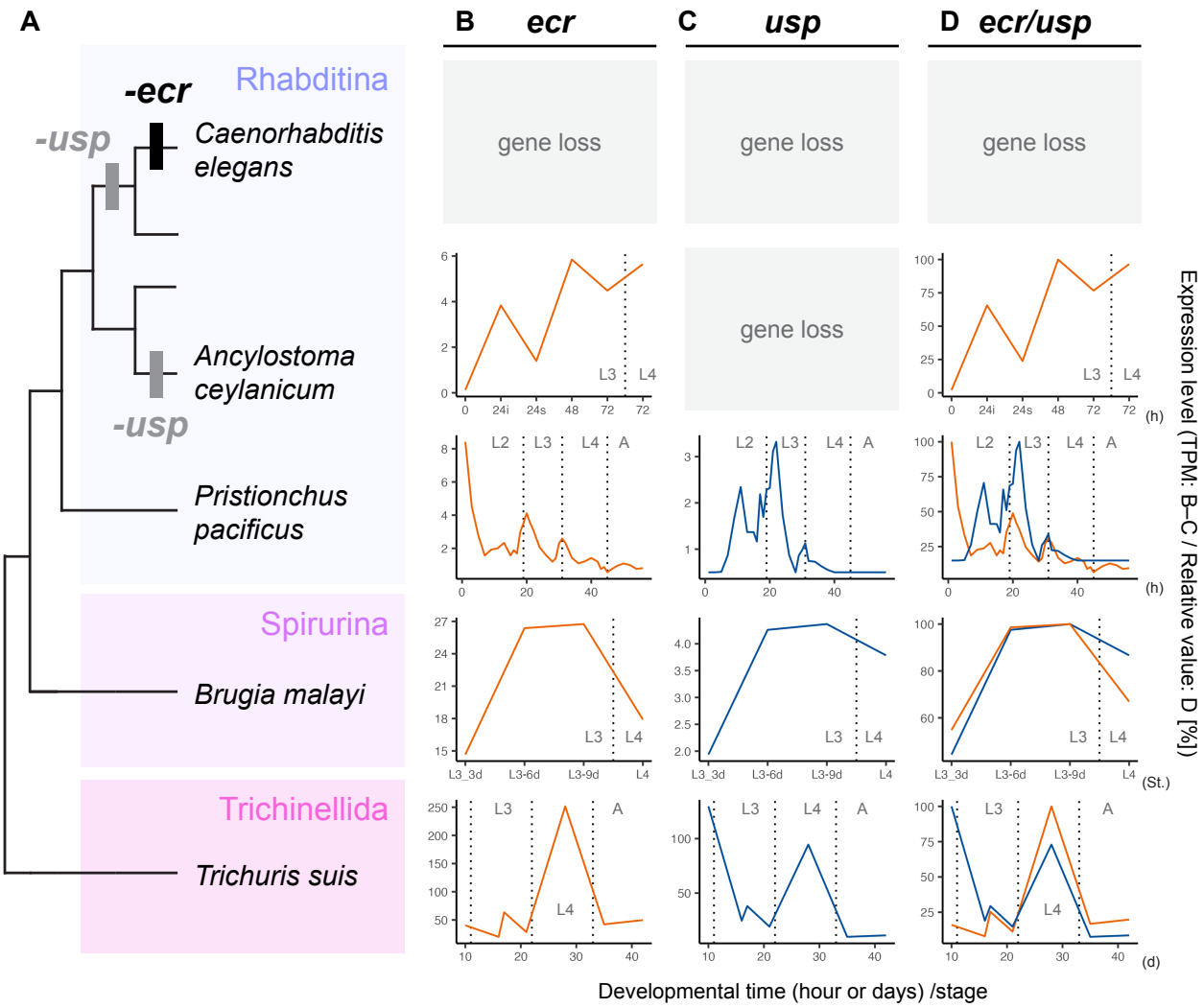
A
B ecr
C usp
D ecr/usp
Rhabditina
-ecr
-usp
Caenorhabditis elegans
Ancylostoma ceylanicum
-usp
Pristionchus pacificus
Spirurina
Brugia malayi
Trichinellida
Trichuris suis
gene loss
gene loss
gene loss
gene loss
L2
L3
L4
A
(h)
(St.)
(d)
L3_3d
L3-6d
L3-9d
Expression level (TPM: B–C / Relative value: D [%])
Developmental time (hour or days) /stage

1417 **Figure 4. Temporal expression pattern of *ecr* and *usp* during the molting cycle in the**
1418 **representative nematode species**
1419 **A**: Phylogeny of the target nematode species and occurrence of *ecr* and *usp* loss events. **B**–
1420 **D**: Temporal expression patterns of *ecr*, *usp,* and both genes, respectively. The x-axis
1421 indicates developmental time (hours/h, days/d, or stages/St.), and the y-axis shows
1422 expression levels (transcripts per million [TPM] in **B** and **C** and relative expression level
1423 [%] in **D**). The vertical dotted lines indicate the timing of molting or ecdysis (L1–L4: first
1424 to fourth larval stages; A: adult stage).
1425

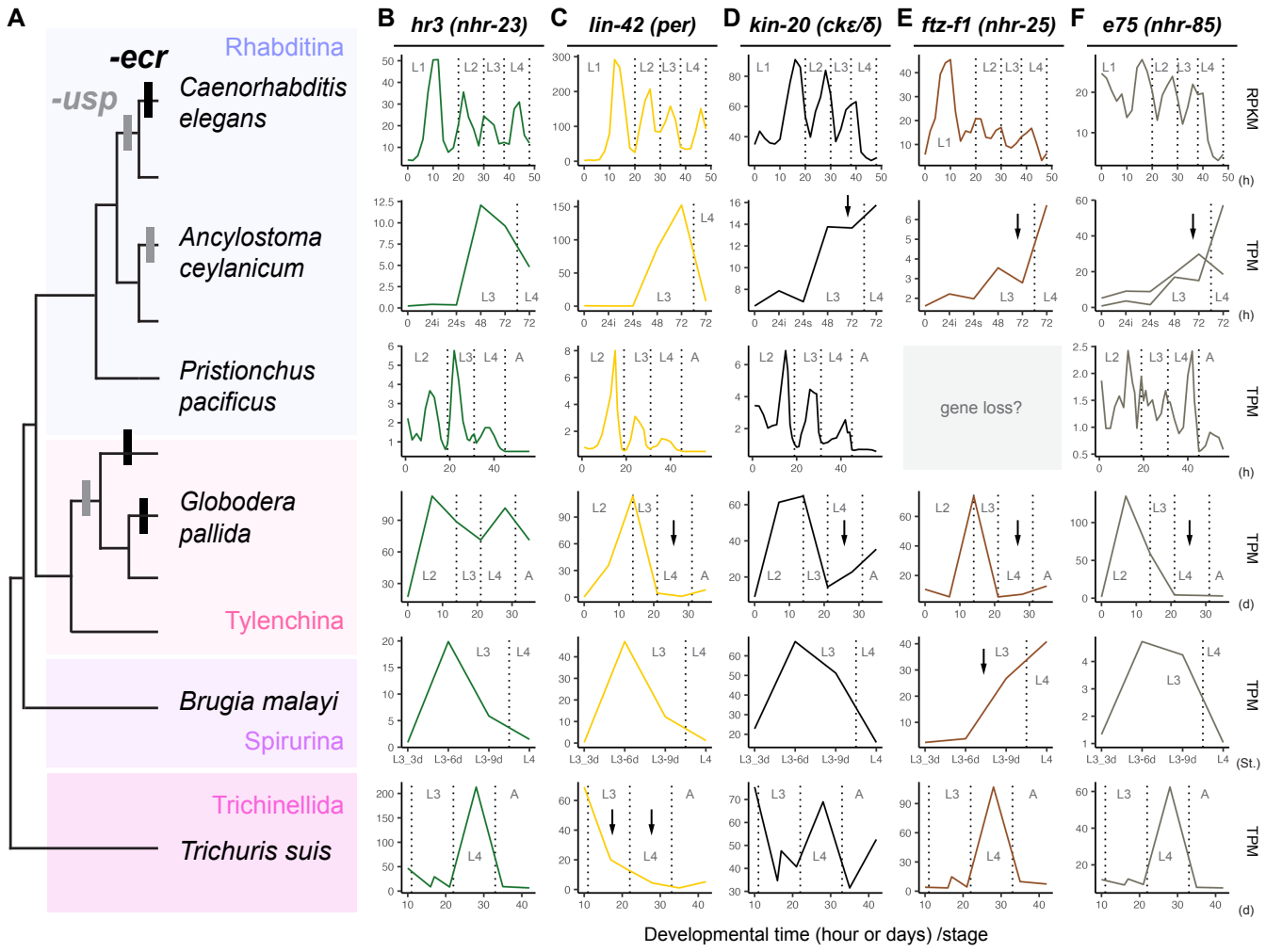
A
-ecr
-usp
Rhabditina
Caenorhabditis elegans
Ancylostoma ceylanicum
Pristionchus pacificus
Globodera pallida
Tylenchina
Brugia malayi
Spirurina
Trichinellida
Trichuris suis
B hr3 (nhr-23)
C lin-42 (per)
D kin-20 (ckε/δ)
E ftz-f1 (nhr-25)
F e75 (nhr-85)
RPKM
TPM
gene loss?
(h)
(d)
(St.)
Developmental time (hour or days) /stage

1426 **Figure 5. Temporal expression pattern of *hr3*, *lin-42*, *kin-20, e75,* and *ftz-f1* during the**
1427 **molting cycle in representative nematode species**
1428 **A**: Phylogeny of the target nematode species and occurrence of *ecr* and *usp* loss events. **B**–
1429 **F**: Temporal expression patterns of *hr3/nhr-23*, *lin-42/per, kin-20/ck1* ε δ, *e75/nhr*-85,
1430 and *ftz-f1/nhr-25* genes, respectively. The x-axis indicates developmental time (hours/h,
1431 days/d, or stages/St.), and the y-axis shows expression levels (RPKM or TPM). The vertical
1432 dotted lines indicate the timing of molting or ecdysis (L1–L4: first to fourth larval stages;
1433 A: adult stage). The arrows indicate that there was no increased or peaked in expression
1434 just before molting/ecdysis.

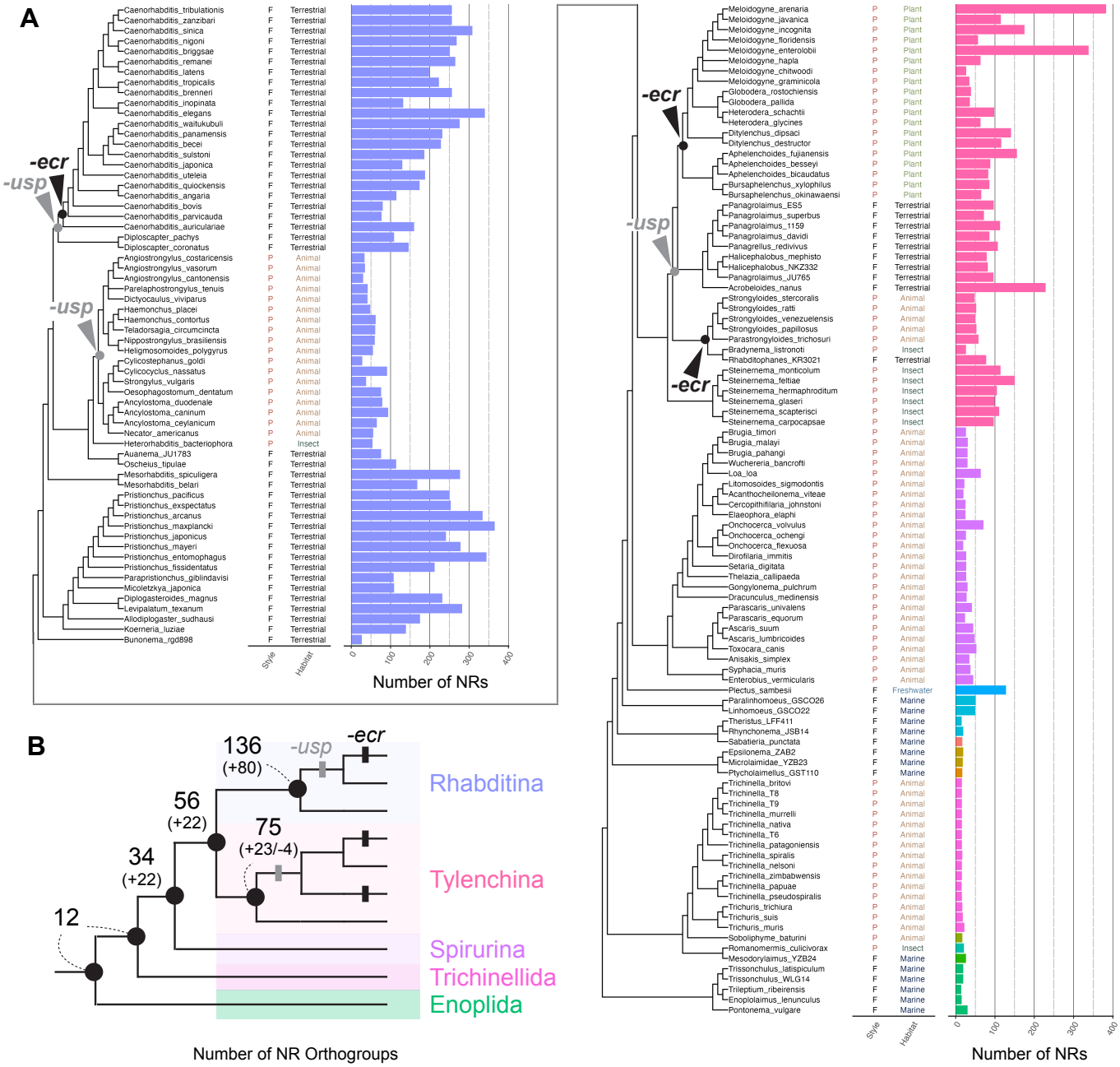
A
-ecr
-usp
-usp
-ecr
Caenorhabditis_tribulationis
Caenorhabditis_zanzibari
Caenorhabditis_sinica
Caenorhabditis_nigoni
Caenorhabditis_briggsae
Caenorhabditis_remanei
Caenorhabditis_latens
Caenorhabditis_tropicalis
Caenorhabditis_brenneri
Caenorhabditis_inopinata
Caenorhabditis_elegans
Caenorhabditis_waitukubuli
Caenorhabditis_panamensis
Caenorhabditis_becei
Caenorhabditis_sulstoni
Caenorhabditis_japonica
Caenorhabditis_uteleia
Caenorhabditis_quiockensis
Caenorhabditis_angaria
Caenorhabditis_bovis
Caenorhabditis_parvicauda
Caenorhabditis_auriculariae
Diploscapter_pachys
Diploscapter_coronatus
Angiostrongylus_costaricensis
Angiostrongylus_vasorum
Angiostrongylus_cantonensis
Parelaphostrongylus_tenuis
Dictyocaulus_viviparus
Haemonchus_placei
Haemonchus_contortus
Teladorsagia_circumcincta
Nippostrongylus_brasiliensis
Heligmosomoides_polygyrus
Cylicostephanus_goldi
Cylicocyclus_nassatus
Strongylus_vulgaris
Oesophagostomum_dentatum
Ancylostoma_duodenale
Ancylostoma_caninum
Ancylostoma_ceylanicum
Necator_americanus
Heterorhabditis_bacteriophora
Auanema_JU1783
Oscheius_tipulae
Mesorhabditis_spiculigera
Mesorhabditis_belari
Pristionchus_pacificus
Pristionchus_exspectatus
Pristionchus_arcanus
Pristionchus_maxplancki
Pristionchus_japonicus
Pristionchus_mayeri
Pristionchus_entomophagus
Pristionchus_fissidentatus
Parapristionchus_giblindavisi
Micoletzkya_japonica
Diplogasteroides_magnus
Levipalatum_texanum
Allodiplogaster_sudhausi
Koerneria_luziae
Bunonema_rgd898
Style
Habitat
0
100
200
300
400
Number of NRs
-ecr
-usp
-ecr
Meloidogyne_arenaria
Meloidogyne_javanica
Meloidogyne_incognita
Meloidogyne_floridensis
Meloidogyne_enterolobii
Meloidogyne_hapla
Meloidogyne_chitwoodi
Meloidogyne_graminicola
Globodera_rostochiensis
Globodera_pallida
Heterodera_schachtii
Heterodera_glycines
Ditylenchus_dipsaci
Ditylenchus_destructor
Aphelenchoides_fujianensis
Aphelenchoides_besseyi
Aphelenchoides_bicaudatus
Bursaphelenchus_xylophilus
Bursaphelenchus_okinawaensi
Panagrolaimus_ES5
Panagrolaimus_superbus
Panagrolaimus_1159
Panagrolaimus_davidi
Panagrellus_redivivus
Halicephalobus_mephisto
Halicephalobus_NKZ332
Panagrolaimus_JU765
Acrobeloides_nanus
Strongyloides_stercoralis
Strongyloides_ratti
Strongyloides_venezuelensis
Strongyloides_papillosus
Parastrongyloides_trichosuri
Bradynema_listronoti
Rhabditophanes_KR3021
Steinernema_monticolum
Steinernema_feltiae
Steinernema_hermaphroditum
Steinernema_glaseri
Steinernema_scapterisci
Steinernema_carpocapsae
Brugia_timori
Brugia_malayi
Brugia_pahangi
Wuchereria_bancrofti
Loa_loa
Litomosoides_sigmodontis
Acanthocheilonema_viteae
Cercopithifilaria_johnstoni
Elaeophora_elaphi
Onchocerca_volvulus
Onchocerca_ochengi
Onchocerca_flexuosa
Dirofilaria_immitis
Setaria_digitata
Thelazia_callipaeda
Gongylonema_pulchrum
Dracunculus_medinensis
Parascaris_univalens
Parascaris_equorum
Ascaris_suum
Ascaris_lumbricoides
Toxocara_canis
Anisakis_simplex
Syphacia_muris
Enterobius_vermicularis
Plectus_sambesii
Paralinhomoeus_GSCO26
Linhomoeus_GSCO22
Theristus_LFF411
Rhynchonema_JSB14
Sabatieria_punctata
Epsilonema_ZAB2
Microlaimidae_YZB23
Ptycholaimellus_GST110
Trichinella_britovi
Trichinella_T8
Trichinella_T9
Trichinella_murrelli
Trichinella_nativa
Trichinella_T6
Trichinella_patagoniensis
Trichinella_spiralis
Trichinella_nelsoni
Trichinella_zimbabwensis
Trichinella_papuae
Trichinella_pseudospiralis
Trichuris_trichiura
Trichuris_suis
Trichuris_muris
Soboliphyme_baturini
Romanomermis_culicivorax
Mesodorylaimus_YZB24
Trissonchulus_latispiculum
Trissonchulus_WLG14
Trileptium_ribeirensis
Enoplolaimus_lenunculus
Pontonema_vulgare
Style
Habitat
0
100
200
300
400
Number of NRs
B
136
(+80)
-usp
-ecr
56
(+22)
75
(+23/-4)
34
(+22)
12
Rhabditina
Tylenchina
Spirurina
Trichinellida
Enoplida
Number of NR Orthogroups

1435 **Figure 6. The evolutionary process of expansion of nematode nuclear receptors**
1436 **A**: Lifestyle (P: parasite and F: free-living), habitat, and the number of nuclear receptors
1437 (NRs) are indicated in the phylogeny of the target nematode species (color represents the
1438 taxa, see Fig. 1B). The nodes of *ecr* and *usp* loss events are highlighted in the tree. **C**: a
1439 simpler tree indicating the increase of NR orthogroups (OGs) at the nodes of representative
1440 taxa. The number above shows the number of OGs, and the number in the brackets below
1441 shows the increase (+) or decrease (-) of OGs at each node.
1442
1443
1444
1445
1446
1447
1448

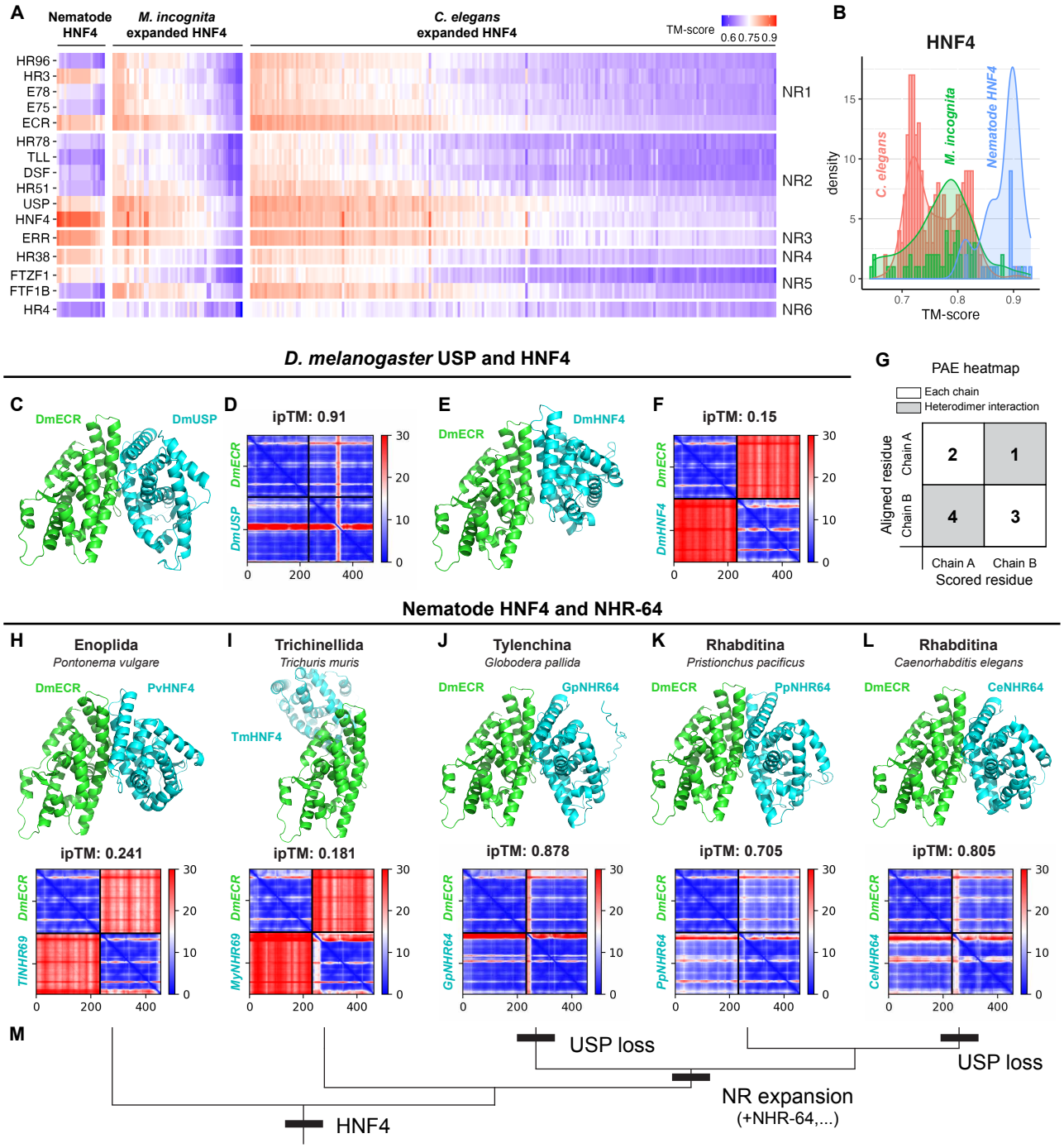
A
Nematode HNF4
M. incognita expanded HNF4
C. elegans expanded HNF4
TM-score
0.6 0.75 0.9
HR96
HR3
E78
E75
ECR
HR78
TLL
DSF
HR51
USP
HNF4
ERR
HR38
FTZF1
FTF1B
HR4
NR1
NR2
NR3
NR4
NR5
NR6
B
HNF4
C. elegans
M. incognita
Nematode HNF4
density
TM-score
D. melanogaster USP and HNF4
C
DmECR
DmUSP
D
ipTM: 0.91
E
DmECR
DmHNF4
F
ipTM: 0.15
G
PAE heatmap
Each chain
Heterodimer interaction
Aligned residue
Chain A
Chain B
Scored residue
Nematode HNF4 and NHR-64
H
Enoplida
Pontonema vulgare
DmECR
PvHNF4
ipTM: 0.241
TlNHR69
I
Trichinellida
Trichuris muris
TmHNF4
ipTM: 0.181
MyNHR69
J
Tylenchina
Globodera pallida
DmECR
GpNHR64
ipTM: 0.878
K
Rhabditina
Pristionchus pacificus
DmECR
PpNHR64
ipTM: 0.705
L
Rhabditina
Caenorhabditis elegans
DmECR
CeNHR64
ipTM: 0.805
M
USP loss
USP loss
NR expansion
(+NHR-64,...)
HNF4

1449 **Figure 7. Structural divergence and the evolution of the heterodimer functionality of**
1450 **nematode HNF4 genes during NR expansion events**
1451 **A**: Heatmap of TM-scores for the pairwise structural alignment of the LBDs between
1452 nematode HNF4 and *Drosophila melanogaster* NR proteins. Each column represents the
1453 results of comparing a specific HNF4 protein from nematodes with each of the 16 *D.*
1454 *melanogaster* NRs (HR96, HR3, E78, etc., shown on the left y-axis). The NRs were also
1455 grouped into the subfamily which is indicated in the right y-axis. "Nematode HNF4"
1456 indicates HNF4 proteins from 20 species of early-branching taxa, such as Enoplida (see
1457 the main text). The center and right panels show the expanded HNF4 proteins extracted
1458 from the species *Meloidogyne incognita* and *Caenorhabditis elegans*, respectively. The x-
1459 axis labels (gene ID or name) are not shown in this heatmap, but a heatmap with labels is
1460 available in the supplementary dataset. **B**: Histogram of the TM score with *D. melanogaster*
1461 HNF4 in the three groups (blue: Nematode HNF4 [proteins from 20 species], *M. incognita*,
1462 and *C. elegans*). **C**–**F**: 3D models, ipTM values, and PAE heatmaps of the highest-scoring
1463 predicted heterodimer structure. All target proteins were investigated with ECR from *D.*
1464 *melanogaster* (DmECR). **C**–**D**: *D. melanogaster* USP (DmUSP), **E–F**: *D. melanogaster*
1465 HNF4 (DmHNF4), **H**: *Pontonema vulgare* HNF4 (PvHNF4), **I**; *Trichuris murris* HNF4
1466 (TmHNF4), **J**: *Globodera pallida* NHR-64 (GpNHR-64), **K**: *Pristionchus pacificus* NHR-
1467 64 (PpNHR-64), and **L**; *Caenorhabditis elegans* NHR-64 (CeNHR-64). The ipTM values
1468 and PAE heatmaps are shown above the ipTM heatmaps. **M**: Phylogenetic tree of five
1469 species (*P. vulgare*, *T. muris*, *G.* pallida, *P. pacificus*, and *C. elegans*) showing the origin
1470 of HNF4 and NR expansion and loss of USP.
1471
1472